JACS
JOURNAL OF THE AMERICAN CHEMICAL SOCIETY
pubs.acs.org/JACS
Article

Increasingly Reversible Na/Cl_2 and Li/Cl_2 Batteries

Guanzhou Zhu, Hongbin Xu, Shuo Wang, Yilin Zhang, Jen-Hung Fang, Tao Dai, Daniel J. Zheng, Weiyin Chen, Heejung Roh, Daniel Wang, Davide Menga, Sunmoon Yu, Haldrian Iriawan, Yang Shao-Horn,* and Ju Li*

Cite This: J. Am. Chem. Soc. 2026, 148, 22673−22686

ABSTRACT: Sodium/chlorine and lithium/chlorine batteries are new types of high-voltage and -capacity batteries reported recently with great potential to be developed into high-energy-density batteries for real-world applications. In this work, we report using cobalt polyphthalocyanine grown on multiwalled carbon nanotubes as the positive electrode in both sodium/chlorine and lithium/chlorine batteries to achieve, for the first time, a stable cycling capacity well exceeding the first discharge capacity in chlorine batteries. We employed various techniques together with theoretical calculations to reveal that cobalt polyphthalocyanine not only facilitates the formation of submicron-sized sodium chloride crystals with excellent electrochemical activity, but also enhances the reversibility of chlorine/chloride redox by forming cobalt−chlorine and sodium−nitrogen bonds during battery cycling. Additionally, cobalt polyphthalocyanine acts as a good storage medium for the chlorine that is formed during battery charging. We also discovered that the metal center can be changed from cobalt to iron and the carbon substrate can be varied from multiwalled carbon nanotubes to graphite for both sodium/chlorine and lithium/chlorine batteries. The chlorine batteries can now operate using only a minimal amount of electrolyte, and we were able to construct a sodium/chlorine battery with ∼150 Wh kg^{-1} or ∼325 Wh L^{-1} full-cell energy density for the first time.

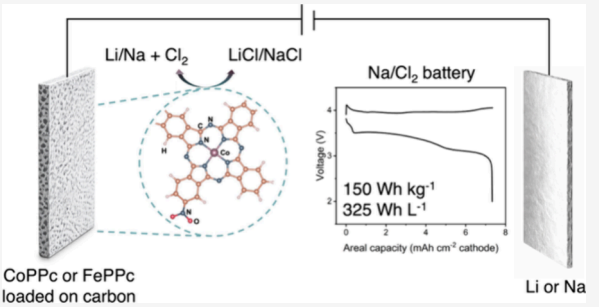

INTRODUCTION

Li-ion batteries have been applied widely in applications ranging from portable electronics such as cell phones and laptops to electric vehicles and emerging electric aviation technologies. With increasing electrification, it is critically important to continue developing rechargeable battery chemistry beyond Li-ion, with low cost, high energy density, and high safety. In 2021, Zhu et al. reported the development of new types of high-voltage, high-capacity rechargeable batteries, namely sodium/chlorine (Na/Cl_2) and lithium/chlorine (Li/Cl_2) batteries, which use amorphous carbon as the positive electrode with nickel foam as the current collector (positive electrode reaction: 2 $Cl^- \leftrightarrow Cl_2 + 2\ e^-$), aluminum chloride ($AlCl_3$) dissolved in thionyl chloride ($SOCl_2$) with fluoride (F^-) additives as the electrolyte, and either Na or Li metal as the negative electrode.[1] After assembly, these batteries discharge first by reducing $SOCl_2$ into sulfur (S), sulfur dioxide (SO_2), and either sodium chloride (NaCl) for Na/Cl_2 battery or lithium chloride (LiCl) for Li/Cl_2 battery.[2−7] After the first discharge, these batteries cycle by utilizing the redox between either NaCl and Cl_2 or LiCl and Cl_2.[1] After the report of the first Na/Cl_2 and Li/Cl_2 batteries, a great interest in this type of batteries has been sparked in the scientific community with a lot of follow-up works being published. For example, in addition to amorphous carbon, various new positive electrode materials with improved cycling capacity and rate performance were identified for both Li/Cl_2 and Na/Cl_2 batteries, including graphite, activated carbon, covalent organic frameworks, metal−organic frameworks, organic nanocages, free-standing carbon, sulfur-functionalized MXene, and bicontinuous-structured carbon.[8−15] Besides positive electrodes, different negative electrode materials including magnesium (Mg) and silicon (Si) were also reported for $SOCl_2$ and Cl_2 batteries.[16,17] Additionally, the performance of the Li/Cl_2 battery at low temperatures was studied, and the battery was operational at a temperature of as low as −80 °C with an improved 5000 mAh g^{-1} capacity, thus outperforming the current state-of-the-art lithium-ion batteries at low temperatures.[18] Furthermore, the mechanism of the Na/Cl_2 battery was studied in greater detail to reveal the reversible formation of carbon−chlorine bonding and graphitic ordering during battery cycling, and other elements such as iodine were also introduced into the Na/Cl_2 battery to further improve the battery's reversible kinetics.[19,20] Lastly, to tackle the corrosion issue of $SOCl_2$, various organic solvents were

Received: February 3, 2026
Revised: May 7, 2026
Accepted: May 12, 2026
Published: June 1, 2026

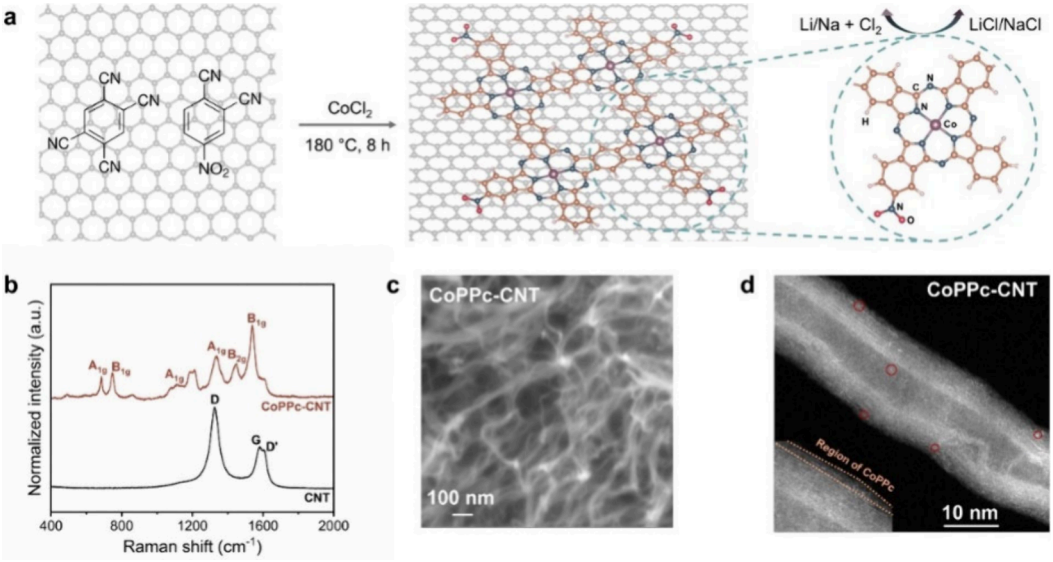

Figure 1. Schematic drawing of the synthesis method for CoPPc-CNT and various characterizations of CoPPc-CNT. (a) Schematic drawing of the synthesis method and the structure of CoPPc-CNT. The key reactions that were supported by CoPPc-CNT in the Cl_2 batteries were also depicted. (b) Raman spectra of CNT and CoPPc-CNT. Characteristic Raman peaks for both CNT and CoPPc were observed in the CoPPc-CNT spectrum (top, red spectrum). (c) SEM image of CoPPc-CNT. The structure of carbon nanotubes was clearly observed. (d) STEM image of CoPPc-CNT. Co sites were indicated by red circles, and CoPPc was observed mostly at the surface of CNT (inset).

identified to replace the $SOCl_2$ while maintaining the Cl^-/Cl_2 chemistry in the battery.[21,22]

Despite all the advancements in the field of Cl_2 batteries, there is still a lot of room for improvement in their performance, especially in further pushing the energy density of the batteries toward practical use. One issue that limits the energy density of the current Cl_2 batteries is their cycling capacity being always much less than the first discharge capacity (typically <50%).[1,8−11,18,19] Such a low utilization of the first discharge capacity can be attributed to the partial irreversible electrolyte reduction during the battery's first discharge to form S, SO_2, and LiCl or NaCl:[1−3]

$$4Na(Li) + 2SOCl_2 \rightarrow S + SO_2 + 4NaCl(LiCl) \quad (1)$$

A low ratio between the cycling capacity and the first discharge capacity (<50%) lowers the practical gravimetric energy densities (~50 Wh kg^{-1} for Na/Cl_2 battery and ~70 Wh kg^{-1} for Li/Cl_2 battery based on previous works[1,8,19]), as an excess of electrolyte is needed in the battery just to support the first discharge capacity (eq 1) and the weight of the electrolyte can easily make up more than 50% of the total weight of all the battery components (~420 mg including negative electrode, positive electrode, separators, and electrolyte).[1,8,18]

Herein, we report a new positive electrode material, namely functionalized cobalt polyphthalocyanine grown on multiwalled carbon nanotubes (denoted as CoPPc-CNT), that can support a cycling capacity (C_{cyc}) well exceeding the first discharge capacity (C_{1DC}) for both Na/Cl_2 and Li/Cl_2 batteries. We employed scanning electron microscopy (SEM) to discover that CoPPc-CNT can facilitate the formation of submicron-sized NaCl crystals during Na/Cl_2 battery discharge with excellent electrochemical activity, leading to high reversibility in the subsequent charging (oxidation of NaCl). In addition, we employed X-ray photoelectron spectroscopy (XPS) together with theoretical calculations to show that the Co center and the pyrrolic N in CoPPc reversibly bond with Cl (Co−Cl) and Na (Na−N) during Na/Cl_2 battery cycling, respectively, facilitating the reversible Cl^-/Cl_2 redox. Moreover, our results from theoretical calculations showed that the adsorption of Cl_2 (formed during battery charging) on CoPPc is stronger than that on pure CNT, making CoPPc a better Cl_2 storage medium than pure CNT. The combination effect of CoPPc being a facilitator for forming submicron-sized NaCl crystals with excellent electrochemical activity, an electrocatalyst for reversible Cl^-/Cl_2 redox, and a great storage medium for Cl_2 leads to an improvement in the Cl_2 batteries reversibility. Lastly, we changed the metal center from Co to iron (Fe) and the carbon substrate from CNT to graphite while maintaining a similar property of $C_{cyc} > C_{1DC}$ for both Na/Cl_2 and Li/Cl_2 batteries. Such a property ($C_{cyc} > C_{1DC}$) increases the practical Cl_2 battery gravimetric and volumetric energy density, where we were able to construct Na/Cl_2 battery with ~150 Wh kg^{-1} and ~325 Wh L^{-1} energy density, calculated based on the mass of all battery components (negative electrode, positive electrode, separator, and electrolyte) and the total volume of the battery pack, including its two electrodes and separator, respectively.

RESULTS AND DISCUSSION

CoPPc-CNT was synthesized by reacting CNT, 4-nitrophthalonitrile, 1,2,4,5-tetracyanobenzene, and cobalt(II) chloride ($CoCl_2$) in an autoclave in 180 °C for 8 h, and the products were centrifuged and washed by ethanol to obtain the final CoPPc-CNT (Figure 1a, Methods). The Na/Cl_2 battery was assembled using Na metal as the negative electrode, CoPPc-CNT loaded on Ni foam as the positive electrode, and $AlCl_3$, NaCl, and sodium bis(fluorosulfonyl)imide (NaFSI) dissolved in $SOCl_2$ as the electrolyte (Methods, Figure S1). Raman spectrum of the CNT that we used for synthesizing CoPPc-CNT displayed 3 characteristic Raman peaks at ~1326 cm^{-1} (D band, disorder-induced), ~1580 cm^{-1} (G band, graphite-like in-plane mode), and ~1605 cm^{-1} (D′ band, in-plane vibrations of outer parts of graphite domains) (Figure

https://doi.org/10.1021/jacs.6c02353
J. Am. Chem. Soc. 2026, 148, 22673−22686

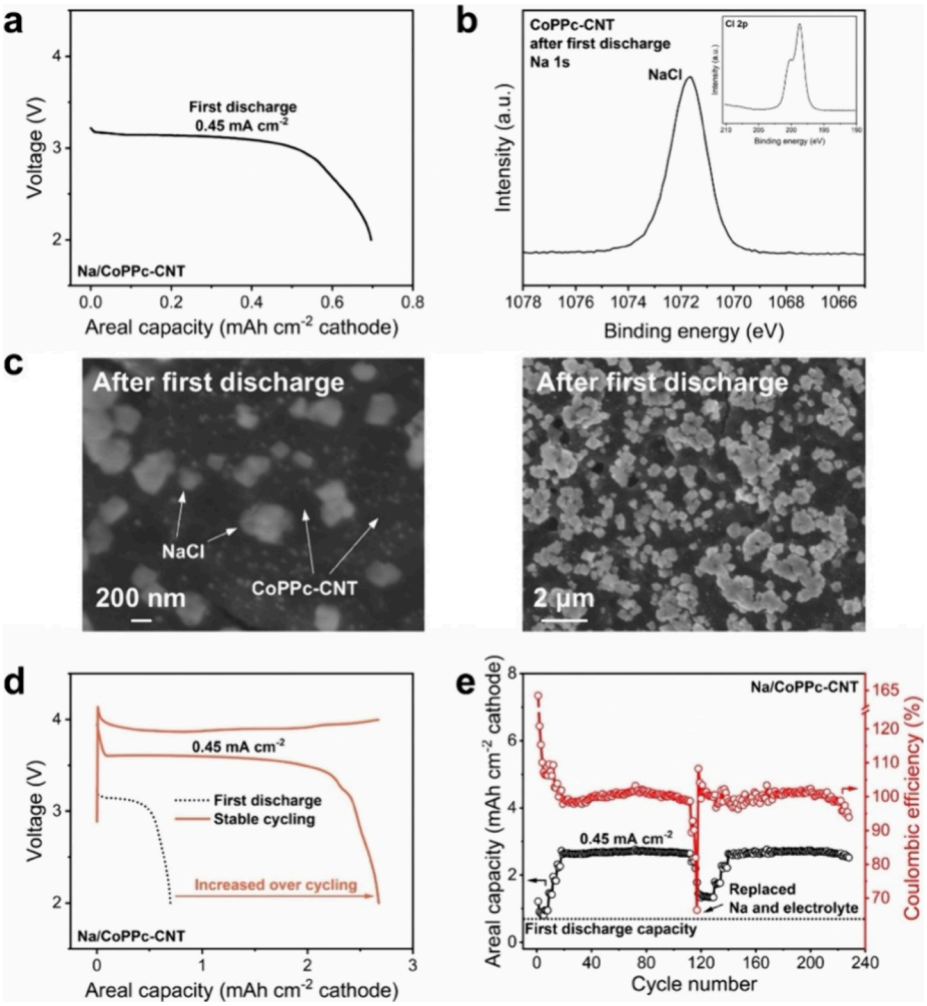

Figure 2. First discharge, charge−discharge, and cycling performance of Na/Cl_2 battery using CoPPc-CNT as the positive electrode and the characterizations of CoPPc-CNT positive electrode after the battery first discharge. (a) First discharge performance of Na/Cl_2 battery with a discharge voltage of ∼3.12 V_{Na} and an areal capacity of ∼0.7 mAh cm^{-2}. (b) Na 1s spectrum of CoPPc-CNT positive electrode after the first discharge. A strong peak at ∼1071.6 eV corresponding to NaCl was observed. Inset: Cl 2p spectrum of CoPPc-CNT positive electrode after the first discharge. A strong peak at ∼198.7 eV (Cl $2p_{3/2}$) corresponding to NaCl was observed. (c) SEM images of CoPPc-CNT after the first discharge. Submicron-sized NaCl crystals (mostly <500 nm, indicated by arrows) were deposited at the electrode and underneath the NaCl crystals were CoPPc-CNT (indicated by arrows). (d) Charge−discharge curve of Na/Cl_2 battery using CoPPc-CNT as the positive electrode with comparison to the first discharge (black, dotted curve). Both the discharge plateau and capacity increased during battery cycling. (e) Cycling performance of Na/Cl_2 battery using CoPPc-CNT as the positive electrode. The battery was able to cycle stably with a cycling capacity that was ∼4 times that of the first discharge capacity. After the Coulombic efficiency began to decay, the cycled CoPPc-CNT electrode could pair with a new Na negative electrode and fresh electrolyte to have the battery cycling recovered. The loading of CoPPc-CNT was ∼4.5 mg cm^{-2}.

1b, black spectrum).[23,24] In comparison, the Raman spectrum of CoPPc-CNT displayed multiple peaks in the range between 400 and 2000 cm^{-1}, in addition to those that were characteristics of CNT, and the spectrum agreed well with previous literature results, suggesting that CoPPc was indeed grown on the CNT substrate (Figure 1b, red spectrum).[25] SEM imaging of CoPPc-CNT clearly revealed its carbon nanotube structures (Figure 1c). Scanning transmission electron microscopy (STEM) of CoPPc-CNT also showed clear carbon nanotubes structures, consistent with SEM image, and bright dots/regions corresponding to Co were also detected (circled in red, Figure 1d). In addition, the region of CoPPc was observed mostly on the surface of CNT (Figure 1d inset). XPS of CoPPc-CNT displayed a strong Co $2p_{3/2}$ peak and Co $2p_{1/2}$ peak at ∼780.8 eV and ∼796.3 eV, respectively, which corresponded to Co in its 2+ oxidation state in CoPPc-CNT (calibrated by C 1s = 284.8 eV, Figure S2a). The N 1s spectrum showed three distinct peaks, one at ∼399 eV (pyridinic N), one at ∼400.2 eV (pyrrolic N), and the last one at ∼406 eV (-NO_2- group), which were the different types of N that were all present in CoPPc-CNT (calibrated by C 1s = 284.8 eV, Figure S2b, Figure 1a).[26,27] All these results suggested that CoPPc-CNT was successfully synthesized and could be further explored as the positive electrode for Na/Cl_2 batteries.

The Na/Cl_2 battery assembled using CoPPc-CNT as the positive electrode had a first discharge voltage of ∼3.12 V_{Na} and an areal capacity of ∼0.7 mAh cm^{-2} (Figure 2a). The reaction occurred during the battery's first discharge was well-known from previous studies to form SO_2, S, and NaCl that was deposited at the positive electrode (eq 1).[1,19] It was estimated that the first discharge capacity of ∼0.7 mAh cm^{-2} only consumed ∼0.74 μL of $SOCl_2$ (eq 1).

https://doi.org/10.1021/jacs.6c02353
J. Am. Chem. Soc. 2026, 148, 22673−22686

XPS of the CoPPc-CNT positive electrode after the first discharge in Na/Cl_2 battery revealed a strong Na 1s peak at ~1071.6 eV, which matched well with the binding energy of Na 1s electrons in NaCl (calibrated by C 1s = 284.8 eV, Figure 2b).[28−30] In addition, Cl 2p spectrum of the CoPPc-CNT electrode after the first discharge displayed a strong Cl $2p_{3/2}$ peak at ~198.7 eV, in agreement with that of NaCl (calibrated by C 1s = 284.8 eV, Figure 2b inset).[30] The S 2p spectrum of the CoPPc-CNT electrode after the first discharge showed the existence of S (formed from $SOCl_2$ reduction, eq 1) and FSI^- (residual electrolyte), further confirming the first discharge reaction (eq 1, Figure S3). SEM imaging of the CoPPc-CNT positive electrode after the first discharge showed the formation of submicron-sized (<500 nm) NaCl crystals together with NaCl nanocrystals (<100 nm) on the electrode (Figure 2c), and underneath these NaCl crystals was CoPPc-CNT, as evidenced by the nonoverlapping signals of Na and C in the SEM/Energy Dispersive X-ray Spectroscopy (EDS) results (Figure S4). In stark contrast, when pure CNT was used as the positive electrode in Na/Cl_2 battery (without CoPPc), after the first discharge, the NaCl particles formed at the CNT electrode were much larger in size (tens of microns) and completely passivated/covered the CNT with no CNT observable by SEM (Figure S5). We believe that these submicron-sized NaCl crystals on CoPPc-CNT had excellent electrochemical activity, i.e., these NaCl crystals were much easier to undergo oxidation in subsequent battery charging, which contributed to the good cyclability of the Na/Cl_2 battery.

In addition, we analyzed CoPPc-CNT electrode after immersing it in Na battery electrolyte for about 6 h using XPS and SEM. The XPS results indicated that NaCl were readily detected, along with other species in the electrolyte such as bis(fluorosulfonyl)imide anion (FSI^-) and aluminum chloride (Figure S6a−e). The Co 2p spectra revealed that no major changes happened to the CoPPc after immersing it in the electrolyte (Figure S6f). Furthermore, sparse NaCl crystals with size of ~200 nm to >1 μm were observed in the SEM images of CoPPc-CNT electrode after immersing in Na battery electrolyte (Figure S7). These results suggested that because NaCl was already present in the electrolyte (Methods), NaCl may also precipitate out from the electrolyte and deposited on the CoPPc-CNT positive electrode along with other species in the electrolyte.

Surprisingly, when the battery entered its cycling stage, the cycling capacity could initially be set at 100% of the first discharge capacity and gradually increased to ~4 times that of the first discharge capacity at ~2.7 mAh cm^{-2} (Figure 2d,e). The main charging plateau of the battery (~3.9 V_{Na}) and the main discharging plateau of the battery (~3.6 V_{Na}) were attributed to the oxidation of NaCl to Cl_2 and the reduction of Cl_2 back to NaCl, respectively.[1,12,19,20]

$$2NaCl \rightarrow 2Na^+ + Cl_2 + 2e^-$$
$$\text{charging, } \sim 3.9\ V_{Na},\ 0.45\ mA\ cm^{-2} \quad (2)$$

$$2Na^+ + Cl_2 + 2e^- \rightarrow 2NaCl$$
$$\text{discharging, } \sim 3.6\ V_{Na},\ 0.45\ mA\ cm^{-2} \quad (3)$$

The main discharge voltage at ~3.6 V_{Na} during cycling was much higher than the first discharge voltage at ~3.12 V_{Na}, which was attributed to a change from reduction of $SOCl_2$ (eq 1) to Cl_2 (eq 3). When cycling at a capacity of at least 100% of the first discharge capacity ($C_{cyc} \geq C_{1DC}$), the Na/Cl_2 battery was able to cycle stably for more than 110 cycles, with the final cycling capacity gradually increased to ~4 times that of the first discharge capacity (Figure 2e). Interestingly, when the battery's Coulombic efficiency began to decay, we could simply replace the cycled Na negative electrode with a new Na negative electrode and added new electrolyte into the battery to continue its cycling (Figure 2e). This suggested that the CoPPc-CNT positive electrode was stable during cycling, and the cycle life of the battery was limited by the stability of the Na negative electrode, making the improvement of Na stability an interesting future research direction. We further performed rate studies on the Na/Cl_2 battery using CoPPc-CNT as the positive electrode, and the battery demonstrated high-rate capability of up to 1 C with an areal capacity of ~3 mAh cm^{-2} (Figure S8).

Additionally, the initial 20 cycles of the Na/Cl_2 battery using CoPPc-CNT as the positive electrode showed Coulombic efficiency of >100% (Figure 2e). Examining the battery's charge−discharge curves of the first 20 cycles revealed that the overpotential, defined as the voltage difference between the main charging and discharging plateaus, decreased from an initial ~0.8 V (cycle 1, ~4.2 V_{Na} charging, ~3.4 V_{Na} discharging, Figure S9) to a stabilized ~0.3 V_{Na} (cycle 50, cycle 60, ~3.9 V_{Na} charging, ~3.6 V_{Na} discharging, Figure S9). Such a decrease in the overpotential was attributed to the 'structural activation' of the CoPPc-CNT positive electrode during the repeated charge−discharge processes, during which the positive electrode underwent possible structural changes (higher surface area/pore volume and more defects) as a result of accommodating all the new species that were generated (ex. Cl_2, SO_2Cl_2, etc.). Note that similar 'activation' phenomenon was also observed in previously reported Cl_2 batteries using carbon-based positive electrode.[8,18] Furthermore, a lower discharging plateau at ~3.1 V_{Na} was observed in all the first 20 cycles of charge−discharge, matching well with the plateau observed in the first discharge (Figure S9). The existence of this plateau suggested that $SOCl_2$ reduction/consumption was still happening in the initial cycling stage of the battery to support the battery's reversible cycling and led to the Coulombic efficiency of >100%. The total capacity contributed by the ~3.1 V_{Na} plateau in the first 20 cycles was ~9.6 mAh, which was much lower than the theoretical capacity of ~55 mAh if all the $SOCl_2$ in the electrolyte was reduced/consumed. This plateau gradually disappeared as the battery entered its stable cycling stage (cycle 50, 60, Figure S9), suggesting that $SOCl_2$ reduction/consumption was no longer happening. As a result, during the initial cycling of the battery, the chemistry within the battery was very dynamic (Cl^-/Cl_2 redox, $SOCl_2$ reduction/consumption, and electrode activation), but when the battery entered its stable cycling stage, the chemistry became less dynamic, and Cl^-/Cl_2 redox became the main redox to support the battery's cycling (Figure S9). The total capacity delivered by the Na/Cl_2 battery using CoPPc-CNT as the positive electrode before replacing the negative electrode (prior to cycle 117, Figure 2e) was ~3 times the theoretical capacity deliverable by reducing all the $SOCl_2$ in the electrolyte (eq 1), suggesting that $SOCl_2$ was the main reactant in the battery only during the first discharge and served as an electrolyte solvent with less and less contribution to the battery's capacity over subsequent cycling.

https://doi.org/10.1021/jacs.6c02353
J. Am. Chem. Soc. 2026, 148, 22673−22686

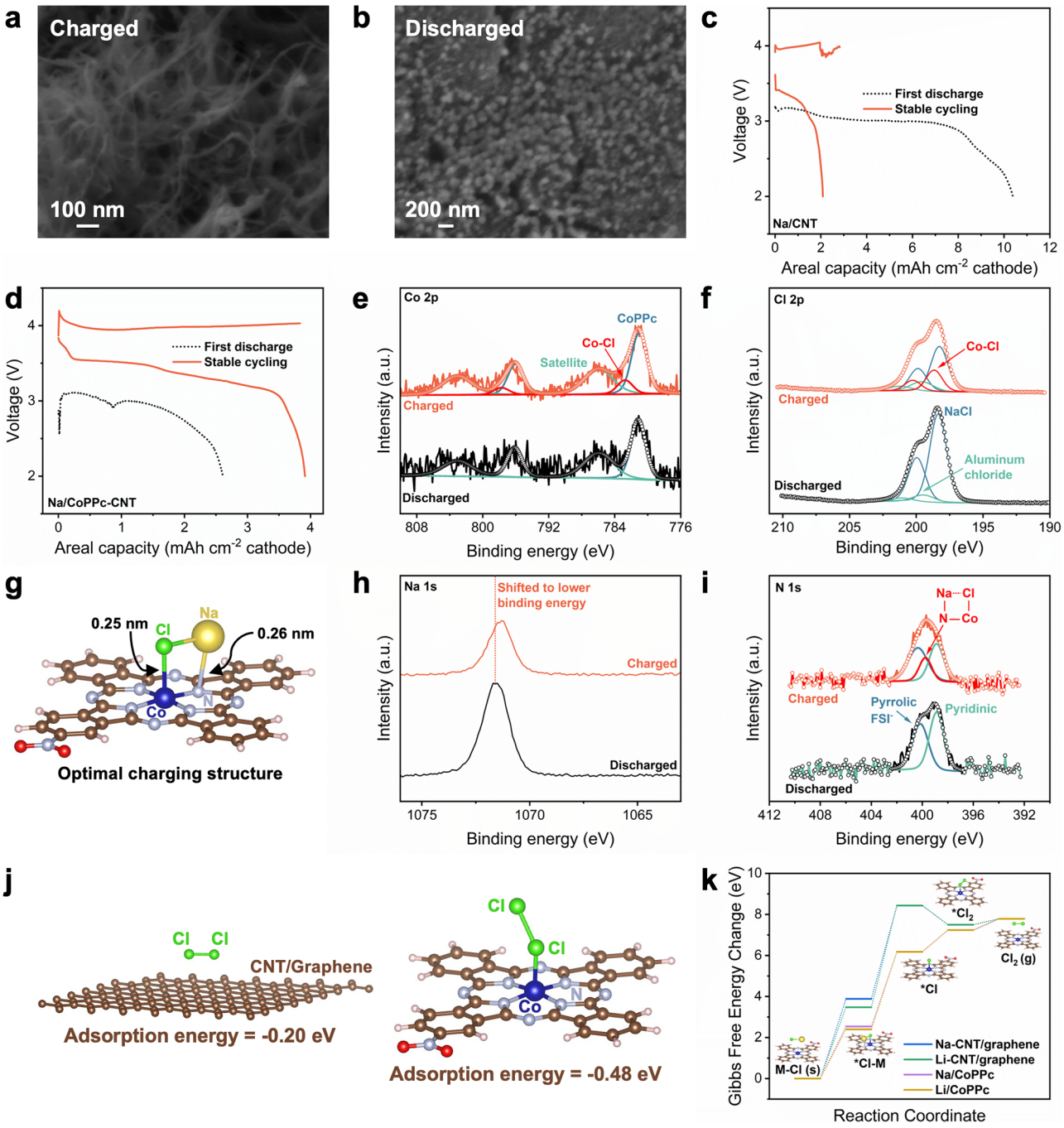

Figure 3. Characterizations and theoretical calculations of CoPPc-CNT and CNT/graphene positive electrodes after charged and discharged in Na/Cl_2 battery and the comparison of Na/Cl_2 batteries using CNT and CoPPc-CNT as the positive electrode. (a) SEM image of charged CoPPc-CNT electrode. The structures of CNT could be easily detected, suggesting the removal of submicron-sized NaCl crystals from the electrode during battery charging. (b) SEM image of discharged CoPPc-CNT electrode. Submicron-sized NaCl crystals were deposited at the electrode and the CNT structures in CoPPc-CNT could no longer be detected. (c) The first discharge curve and charge−discharge behavior of Na/Cl_2 battery using CNT as the positive electrode. The first discharge capacity for the battery was high (~10.4 mAh cm^{-2}), but the battery demonstrated poor cyclability at a cycling capacity ~20.1% of the first discharge capacity. The loading of CNT was ~6.3 mg cm^{-2} with current density of ~3.2 mA cm^{-2}. (d) The first discharge curve and charge−discharge behavior of Na/Cl_2 battery using CoPPc-CNT as the positive electrode. The battery demonstrated a cycling capacity ~150% of the first discharge capacity (C_{cyc}/C_{1DC} = 150%). The loading of CoPPc-CNT was ~6.4 mg cm^{-2}, with current density of ~3.2 mA cm^{-2}. The cycling capacity was gradually increased from 100% to 150% of the first discharge capacity. (e) Co 2p XPS spectra of charged and discharged CoPPc-CNT electrodes. In the charged electrode, a Co−Cl peak existed, suggesting the formation of Co−Cl bonds during battery charging. This peak disappeared when the battery was discharged. The XPS spectra were calibrated by C 1s = 284.8 eV. (f) Cl 2p XPS spectra of charged and discharged CoPPc-CNT electrodes. In the charged electrode, a peak corresponding to Co−Cl bonds was detected, consistent with the Co 2p XPS spectra. The XPS spectra were calibrated by C 1s = 284.8 eV. (g) Optimal structure obtained from theoretical calculations between CoPPc-CNT and NaCl during charging. The structure showed that Co was bonded with Cl (bond length = 0.25 nm) and Na was bonded with N (bond length = 0.26 nm). (h) Na 1s XPS spectra of charged and discharged CoPPc-CNT electrodes. The Na 1s peak shifted to lower binding energy when the battery was charged, suggesting the weakening of the Na−Cl bond and the formation of Na−N bond. The XPS spectra were calibrated by C 1s = 284.8 eV. (i) N 1s XPS spectra of charged and discharged CoPPc-CNT electrodes. In the charged spectrum, one

https://doi.org/10.1021/jacs.6c02353
J. Am. Chem. Soc. 2026, 148, 22673−22686

Figure 3. continued

extra peak corresponding to the pyrrolic N bonded to both Na and Co−Cl was observed. The XPS spectra were calibrated by C 1s = 284.8 eV. (j) Adsorption energy obtained from theoretical calculations when Cl_2 was adsorbed on CNT/graphene (−0.20 eV) versus on CoPPc (−0.48 eV). A lower adsorption energy/stronger adsorption was obtained between Cl_2 and CoPPc. (k) Reaction coordinate and the change in Gibbs Free Energy at each step along the reaction pathway obtained from theoretical calculations. The energy barrier at the rate-limiting step (*Cl-M to *Cl) on CoPPc-CNT positive electrode was lower than that on CNT/graphene positive electrode.

To understand how CoPPc-CNT was able to fully support the reversible cycling of the Na/Cl_2 battery, we first examined the CoPPc-CNT positive electrode stopped at charged and discharged states during battery cycling using SEM. When the battery was charged, the submicrometer-sized NaCl crystals were no longer detected. Instead, the structure of CNT was clearly observed (Figure 3a), indicating that NaCl was oxidized/removed during the charging process (eq 2).[1,12,19,20] When the battery was discharged, submicrometer-sized NaCl crystals were once again detected at the electrode, indicating that NaCl was reversibly formed, mostly from the reduction of Cl_2 (eq 3, Figure 3b, Figure S10).[1,12,19] These submicrometer-sized NaCl crystals were formed both during the first discharge (low capacity, Figure 2a) and during stable cycling (much-improved capacity, Figure 2d,e). Therefore, the formation of these submicrometer-sized NaCl was not a result of the initial low capacity but rather a result of the CoPPc-CNT electrode material. We believe that CoPPc-CNT could provide more nucleation sites that facilitated the formation of submicrometer-sized NaCl crystals (<500 nm), which led to more surfaces per weight of NaCl and helped improve the NaCl oxidation kinetics. Similar but less reversible oxidation/removal and reduction/formation of NaCl (in Na/Cl_2 battery) and LiCl (in Li/Cl_2 battery) at the positive electrode were also observed in previous works on Cl_2 batteries, further validating the above-proposed reactions (eqs 2 and 3).[1,8−12,18,19]

We believe that one of the main reasons allowing the CoPPc-CNT in Na/Cl_2 battery to support a cycling capacity exceeding the first discharge capacity was the ability to form these submicron-sized NaCl crystals during battery discharge (Figures 2c and 3b). When compared with micron-sized NaCl crystals, submicron-sized NaCl crystals were much easier to undergo electrochemical oxidation in forming Cl_2 (eq 2), attributed to a larger surface per weight of NaCl that led to a faster oxidation kinetics and an improved reversibility. Indeed, we compared the cycling capacity versus first discharge capacity of the CNT that we used for growing CoPPc with CoPPc-CNT as the positive electrode in a Na/Cl_2 battery by assembling two identical batteries, with the only difference being the positive electrode materials (same batch and same 50 μL of electrolyte, same separator, same Na negative electrode, ∼2% in mass difference of the positive electrode, Methods). The Na/Cl_2 battery using CNT as the positive electrode demonstrated worse cyclability, as it could only perform charge−discharge with a Coulombic efficiency of ∼74% at a cycling capacity ∼20.1% of the first discharge capacity (cycling capacity/first discharge capacity = 20.1%, Figure 3c). In stark contrast, the Na/Cl_2 battery using CoPPc-CNT as the positive electrode demonstrated a stable charge−discharge performance with a Coulombic efficiency of ∼100% at a cycling capacity ∼150% of the first discharge capacity (cycling capacity/first discharge capacity = 150%, Figure 3d). These results clearly demonstrated the advantage of having a cycling capacity exceeding the first discharge capacity, as the battery did not initially require an excess of electrolyte to satisfy its first discharge capacity. Instead, the consumption of electrolyte during the first discharge was minimal, and only the amount of electrolyte required to support battery cycling was needed inside the battery (50 μL in this case). In fact, because of cycling capacity exceeding the first discharge capacity, the Na/Cl_2 battery using CoPPc-CNT as the positive electrode was able to cycle at a much higher capacity than the battery using CNT as the positive electrode (Figure 3c,d). To the best of our knowledge, using 50 μL of electrolyte to support Cl_2 batteries cycling was a record low, as previous reports on Cl_2 batteries all used at least 100 μL of electrolyte in the battery assembly.[1,8,9,12,18−20]

To mitigate the reduction/consumption of $SOCl_2$ during the initial cycling of Na/Cl_2 battery (Figure S9), we tried predepositing NaCl into CoPPc-CNT in a 1 to 1 mass ratio and used this material as the positive electrode in Na/Cl_2 battery. The resulting Na/Cl_2 battery skipped its first discharge and underwent charge−discharge directly, but the battery behavior was similar to that using CoPPc-CNT as the positive electrode, i.e., the discharge curve after first charging still displayed a main discharging plateau at ∼3.1 V_{Na} ($SOCl_2$ reduction, Figure S11a black dotted curve). Additionally, the battery underwent a similar "activation" process, as evidenced by its initial Coulombic efficiency of >100% and its main discharging plateau gradually increased to ∼3.5 V_{Na} (Figure S11). Our results indicated that simply mixing NaCl and CoPPc-CNT together did not help the battery suppress $SOCl_2$ consumption/reduction. It may be possible that the predeposited NaCl was different from the NaCl that was formed in situ by reducing $SOCl_2$ during battery discharging, in terms of their size and electrochemical activity. We believe that predepositing NaCl or even LiCl is still an interesting and promising idea for explorations in the future. With optimized synthesis conditions, the predeposited NaCl or LiCl may resemble those that were formed in situ during battery cycling. As a result, $SOCl_2$ consumption/reduction can be suppressed, and the battery performance can be improved.

We further employed XPS to examine the CoPPc-CNT electrode stopped at charged and discharged state during battery cycling. Co 2p spectrum of a CoPPc-CNT electrode in discharged state showed an obvious Co $2p_{3/2}$ peak at ∼781 eV, suggesting Co in its 2+ oxidation state that was present in CoPPc (calibrated by C 1s = 284.8 eV, Figure 3e). Another peak at ∼796 eV was also observed, which was attributed to the Co $2p_{1/2}$ peak from the same Co species (Figure 3e). Two broad peaks that were observed at ∼786 and 803 eV were the satellite peaks (Figure 3e). When the CoPPc-CNT electrode was charged, in addition to all the peaks that were detected in a discharged electrode, another pair of peaks at ∼782.7 eV and ∼797.7 eV were observed, which were attributed to the Co $2p_{3/2}$ and Co $2p_{1/2}$ peaks of Co bonded with Cl (Co−Cl, Figure 3e). Such Co−Cl bonding was only observed in a charged state electrode and not in a discharged state electrode, suggesting that the bonding between Co and Cl was highly reversible. Cl 2p spectra of charged and discharged CoPPc-

https://doi.org/10.1021/jacs.6c02353
J. Am. Chem. Soc. 2026, 148, 22673−22686

CNT electrodes showed similar phenomena. In the discharged CoPPc-CNT, its Cl 2p spectrum only depicted two sets of peaks, one set at ∼198.4 eV and ∼200 eV, corresponding to Cl $2p_{3/2}$ and Cl $2p_{1/2}$ peaks of Cl in NaCl,[31] and another set at ∼199.5 eV and ∼201.1 eV, corresponding to Cl $2p_{3/2}$ and Cl $2p_{1/2}$ peaks of Cl in aluminum chloride that was present in the electrolyte (calibrated by C 1s = 284.8 eV, Figure 3f, Methods).[32] In contrast, when the CoPPc-CNT electrode was charged, in addition to the peaks corresponding to NaCl and aluminum chloride, another set of peaks at ∼198.7 eV and ∼200.3 eV was detected, attributed to the Cl $2p_{3/2}$ and Cl $2p_{1/2}$ peaks of Cl in Co−Cl bonds (Figure 3f). We employed theoretical calculations to simulate the optimal structure between NaCl and CoPPc-CNT during charging, and our result confirmed the formation of Co−Cl bond, with a bond length of ∼0.25 nm (Figure 3g). Interestingly, our theoretical calculations also showed that Na would bond with the pyrrolic N in CoPPc-CNT with a bond length of ∼0.26 nm (Na−N, Figure 3g). In fact, our Na 1s and N 1s XPS results were consistent with our theoretical calculations. The Na 1s peak of a charged CoPPc-CNT electrode showed a shift to a lower binding energy of ∼1071.3 eV when compared to the Na 1s peak at ∼1071.6 eV of a discharged CoPPc-CNT electrode (calibrated by C 1s = 284.8 eV, Figure 3h). Such a shift was explained by the weakening of Na−Cl bond together with the formation of Co−Cl and Na−N bonds as a result of NaCl oxidation (eq 2), leading to an overall more partial negative charge on the Na and causing the Na 1s electrons to have a lower binding energy. Lastly, the N 1s spectra also showed a significant difference between discharged and charged CoPPc-CNT electrodes (calibrated by C 1s = 284.8 eV, Figure 3i). In the discharged electrode, the N 1s spectrum consisted of two peaks, one at ∼399 eV, corresponding to pyridinic N, and the other at ∼400.2 eV, corresponding to a mixture of FSI^- anions (parts of the electrolyte, Methods) and pyrrolic N (Figure 3i).[33,34] In contrast, the N 1s spectrum of the charged CoPPc-CNT electrode displayed three peaks (Figure 3i). In addition to the two peaks at ∼399.0 eV and ∼400.2 eV that were also present in the discharged electrode, a new peak at ∼399.8 eV was observed, which was assigned to the original pyrrolic N now bonded with both Na and Co−Cl (Figure 3i, Na−N−Co-Cl indicated by red arrow). When Co bonded with Cl, Co became more partial positive due to the electronegativity of Cl (Figure 3e), and a more partial positive Co would make the N bonded to it more partial negative. In addition, N bonded with Na could also make the N bear a more partial negative charge. All these interactions led to the lowering of the N 1s electrons' binding energy from the original ∼400.2 eV (pyrrolic N) to ∼399.8 eV (Na−N−Co-Cl, Figure 3i). Besides Co 2p, Cl 2p, Na 1s, and N 1s, all other relevant elements (C 1s, Al 2p) showed almost identical XPS spectra between the charged and discharged CoPPc-CNT electrodes, suggesting that the key changes indeed happened to the CoPPc material (Figure S12).

The bonding between Co and Cl during charging not only facilitated the oxidation of NaCl, but also helped push the cycling capacity of the battery to higher than the first discharge capacity. When the Cl in NaCl bonded with Co, the bonding between Na and Cl was weakened, thus leading to an easier oxidation of NaCl. Additionally, when compared with NaCl that loosely covered the positive electrode, NaCl that interacted with the positive electrode, such as forming chemical bonds with the positive electrode, were more electrochemically active and could undergo oxidation much easier. We examined the charge−discharge curves of two consecutive cycles in Na/Cl_2 battery using CoPPc-CNT as the positive electrode: in one cycle the battery was cycling normally (Figure S13 red solid curve), and in the other cycle the cycling capacity was increased (Figure S13 blue dotted curve). During cycling (Figure S13 red solid curve), the main charging plateau at ∼3.9 V_{Na} was attributed to the oxidation of NaCl to Cl_2 (eq 2). Toward the end of charging, the charging plateau raised to a higher voltage of ∼4 V_{Na}, attributed to the oxidation of $SOCl_2$:[1,2,19]

$$SOCl_2 + SOCl^+AlCl_4^- + 2AlCl_4^- \rightarrow SCl(AlCl_4) + SO_2Cl_2 + Cl_2 + 2AlCl_3 + 2e^- \quad (4)$$

In eq 4, $SOCl^+AlCl_4^-$ was formed when $AlCl_3$ was added into and reacted with $SOCl_2$ (methods), and $SCl(AlCl_4)$ was a complex formed between SCl_2 and $AlCl_3$.[2,19]

When the cycling capacity was increased (Figure S13 blue dotted curve), the charging curve traced its previous cycle and the charging voltage continued to increase toward the end, as a result of more electrolyte oxidation (Figure S13 blue dotted curve, eq 4). During discharging, the main discharging plateau was extended (more Cl_2 reduction, Figure S13 blue dotted curve, eq 3), due to the formation of more Cl_2 during charging (eq 2, 4). Additionally, an extension of the plateau at ∼3.2 V_{Na} was observed, attributed to the reduction of SO_2Cl_2 formed during charging ($SOCl_2$ oxidation, eq 4):[1,2,18,19]

$$2Na + SO_2Cl_2 \rightarrow SO_2 + 2NaCl \quad (5)$$

We proposed that the bonding between Co and Cl could help the oxidation of Cl^- originating from both NaCl (eq 2) and $SOCl_2$ (eq 4) to Cl_2, leading to an excellent reversibility during battery cycling even when the cycling capacity was increased and more electrolytes were oxidized. In fact, the second cycle, right after the capacity was increased, displayed a more dominant NaCl oxidation during charging and less electrolyte oxidation toward the end of charging (Figure S13 green solid curve). Consequently, the subsequent discharging step showed more Cl_2 reduction and less SO_2Cl_2 reduction (Figure S13 green solid curve vs blue dotted curve), suggesting that the battery's mechanism shifted more toward the redox between NaCl and Cl_2. The formation of both the Na−N and Co−Cl bonding led to a stronger interaction between the NaCl and the positive electrode, thus making the NaCl more electrochemically active and easier to undergo oxidation to form Cl_2. Such a facile and reversible redox between NaCl and Cl_2 allowed the battery to have a cycling capacity exceeding the first discharge capacity and was also the reason why the battery's main reaction could shift back to the redox between NaCl and Cl_2 (eq 2, 3) from electrolyte oxidation (eq 4) shortly after the cycling capacity was increased (Figure S13 green solid curve vs blue dotted curve).

Furthermore, we purposefully made the capacity increase in the initial cycling of the Na/Cl_2 battery to follow a stepwise and gradual setting, i.e., the capacity was slowly increased over multiple steps instead of suddenly raised to the target capacity (Figure 2e). The reason was to minimize $SOCl_2$ oxidation and electrolyte consumption during this capacity increase process (eq 4). A small amount of $SOCl_2$ oxidation and electrolyte consumption would occur every time when the charging capacity was raised to be higher than the previous discharging capacity, as evidenced by the extension of the charging plateau at ∼4 V_{Na} (Figure S13 blue dotted curve, eq 4), leading to a

https://doi.org/10.1021/jacs.6c02353
J. Am. Chem. Soc. 2026, 148, 22673−22686

small perturbation to the battery electrolyte chemistry. When the charging capacity increase was gradual, such perturbation was small and had minimal effect on the battery stable cycling. However, if the charging capacity was increased abruptly to the target capacity, a lot of $SOCl_2$ oxidation and electrolyte consumption would happen at once to fulfill the sudden capacity increase (eq 4, Figure S13), which would lead to a severe perturbation of the battery electrolyte chemistry and cause the battery cycling to decay much more rapidly.

We also employed theoretical calculations to examine the adsorption energy of Cl_2* (*: adsorbed) on both CNT/graphene and CoPPc. Our results indicated that Cl_2* had a lower adsorption energy/stronger adsorption with CoPPc (adsorption energy = −0.48 eV) than with CNT/graphene (adsorption energy = −0.20 eV, Figure 3j). This result indicated that CoPPc acted as a better storage medium for Cl_2 than CNT, attributed to its ability in forming Co−Cl bonding that may improve the stability of Cl_2* (Figure 3e,f,g,j). Because of its better Cl_2 storage ability, CoPPc-CNT was able to support higher cycling capacity than CNT when used as the positive electrode in a Na/Cl_2 battery (Figure 3c,d). Additionally, the Cl_2 storage/adsorption ability of CoPPc-CNT allowed Cl_2 to be well-confined within the positive electrode material and thus making the battery safe to operate. The electrolyte that we used (mostly $SOCl_2$) should also have solubility toward different gaseous species that were generated during batteries cycling (SO_2, Cl_2, etc.), further alleviating the concern of pressure built up within the batteries.[35] In fact, among all the coin cell batteries that we assembled, we did not observe any battery explosion as a result of pressure built up within the battery. Moreover, when the batteries were stopped in the discharged state, no more Cl_2 was present inside the battery, as Cl_2 was reduced to form either LiCl (Li/Cl_2 battery) or NaCl (Na/Cl_2 battery). With the presence of LiCl or NaCl, the batteries recycling process would also be less challenging. We propose that the oxidation of metal chloride (M−Cl, Figure 3k) to Cl_2 followed a reaction pathway in which the metal chloride was first converted to *Cl (Cl bonded with the positive electrode, *: CoPPc or CNT/graphene positive electrode, Figure 3k) and then two *Cl eventually formed *Cl_2 (Cl_2 adsorbed on the positive electrode, Figure 3k). Our theoretical calculations revealed that the energy barrier at the rate-limiting step in our proposed reaction pathway (*Cl−M to *Cl, *: CoPPc or CNT/graphene, Figure 3k) was lower on CoPPc-CNT positive electrode than that on CNT/graphene positive electrode (Figure 3k), and such a lower energy barriers made the oxidation of metal chloride on CoPPc more energetically favored and facile than that on CNT/graphene, leading to the improved cyclability at a cycling capacity exceeding the first discharge capacity when CoPPc-CNT was used as the positive electrode in Na/Cl_2 battery. The reaction intermediates in our proposed reaction pathway (Figure 3k) were also consistent with our experimental XPS results (Figure 3e,f,h,i). The DFT energy, TΔS+ZPE corrections, and Gibbs energy were also tabulated (Table S1). In addition, we further validated our theoretical calculations by using different exchange-correlation functionals, including RPBE (Figure S14a, Table S2),[36] Bayesian error estimation functional with van der Waals correlation (BEEF-vdW, Figure S14b, Table S3),[37] and r^2SCAN+rVV10 (Figure S14c, Table S4).[38,39] Our results indicated that the proposed reaction pathway remained consistent regardless of which functionals we used, further validating our proposed reaction mechanism. The difference between the CoPPc-CNT and CNT electrodes in facilitating the redox between Cl^- and Cl_2 could also be seen by comparing the charge−discharge curves of the Na/Cl_2 battery using CoPPc-CNT (Figure 2d) and CNT (Figure 2c) as the positive electrodes (Figure S15). The battery using CoPPc-CNT as the positive electrode demonstrated much lower overpotential (∼0.45 V, defined as the voltage difference between the charging and discharging plateaus) than the battery using CNT as the positive electrode (∼0.70 V, Figure S15). This suggested that the Cl_2/Cl^- redox was much more sluggish on CNT than on CoPPc-CNT, attributed to a much weaker interaction/adsorption of Cl_2 on CNT than on CoPPc-CNT and a more facile redox kinetics of the submicron-sized NaCl formed on CoPPc-CNT (Figure 2b), consistent with the results from theoretical calculations (adsorption energy of Cl_2 on CoPPc-CNT: −0.48 eV, adsorption energy of Cl_2 on CNT: −0.20 eV, Figure 3j). The ability to form chemical interactions between NaCl and CoPPc, i.e., the formation of Co−Cl and Na−N bonds, was also a unique feature to the CoPPc-CNT electrode, as all the previously reported Cl_2 batteries using carbon-based positive electrodes demonstrated only physical interaction/adsorption between the active materials (NaCl, LiCl, Cl_2, etc.) and the positive electrode.

Furthermore, we compared the chlorine evolution performance of CoPPc-CNT and CNT using a three-electrode setup (working electrode: CoPPc-CNT or CNT on carbon fiber paper, counter electrode: platinum foil, and reference electrode: reversible hydrogen electrode). The electrolyte that we used was either 0.05 M sulfuric acid (H_2SO_4) and 0.10 M NaCl in deionized water (for the chlorine evolution reaction) or 0.05 M H_2SO_4 and 0.10 M sodium perchlorate ($NaClO_4$) in deionized water (for the oxygen evolution reaction). Our CV results indicated that CoPPc-CNT and CNT demonstrated very similar performance for the oxygen evolution reaction (Figure S16a, dotted curves). However, they demonstrated clear differences for the chlorine evolution reaction, with CoPPc-CNT showing a much higher current than CNT at the same potential (Figure S16a, solid curves). The Tafel slopes of chlorine evolution after subtracting the current from oxygen evolution reaction for both CoPPc-CNT and CNT were analyzed (Methods), and our results indicated that CoPPc-CNT was a much better catalyst for chlorine evolution than CNT, with a lower onset potential and a smaller Tafel slope (Figure S16b), consistent with our proposed reaction mechanism. Additionally, the rate-determining step in our proposed reaction pathway involved the transfer of one electron (Figure 3k and Figure S16b), corresponding to a Tafel slope of 60 mV dec^{-1}. The Tafel slope of 65.3 mV dec^{-1} obtained for CoPPc-CNT was also consistent with the rate-limiting step in our proposed reaction pathway. We believe that the combination effect of CoPPc being a facilitator for the formation of submicrometer-sized NaCl crystals with excellent electrochemical activity, an electrocatalyst for reversible Cl^-/Cl_2 redox, and a good Cl_2 storage medium led to the resulting Na/Cl_2 battery using CoPPc-CNT as the positive electrode being able to cycle at a capacity exceeding the first discharge capacity.

We performed Raman spectroscopy analysis on the cycled CoPPc-CNT electrode stopped at different states during Na/Cl_2 battery cycling (Figure S17a). The major Raman peaks in pristine CoPPc-CNT were also readily detected in cycled CoPPc-CNT, suggesting that no major structural change/

https://doi.org/10.1021/jacs.6c02353
J. Am. Chem. Soc. 2026, 148, 22673−22686

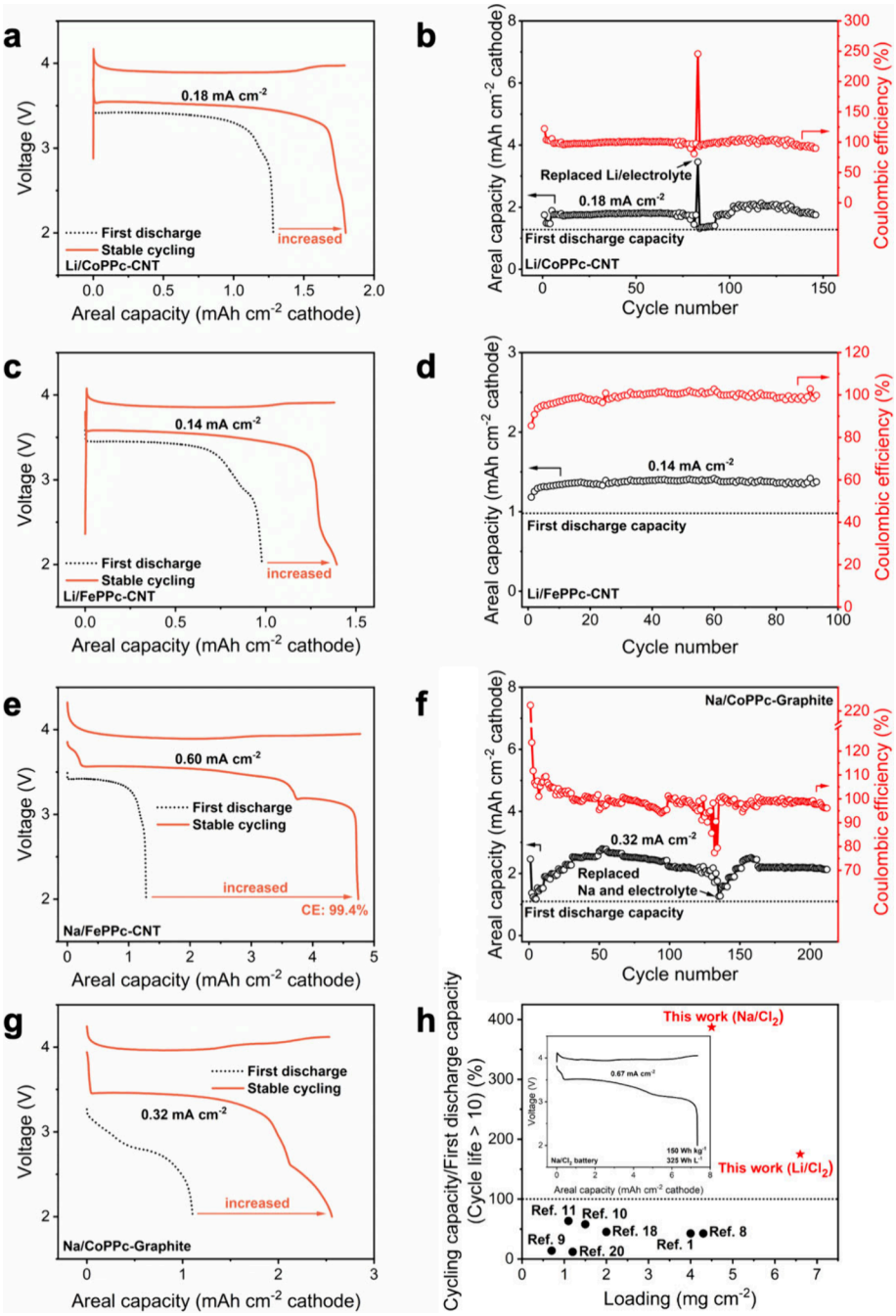

Figure 4. Na/Cl_2 and Li/Cl_2 battery performances using CoPPc-CNT, FePPc-CNT, and CoPPc-Graphite as the positive electrode and comparison of CoPPc-CNT positive electrode in Na/Cl_2 and Li/Cl_2 batteries with previous reported literatures. (a) The first discharge curve and charge−discharge behavior of Li/Cl_2 battery using CoPPc-CNT as the positive electrode. The resulting Li/Cl_2 battery was able to stably cycle at a capacity higher than the first discharge capacity with a higher discharge voltage (cycling capacity/first discharge capacity = 140%). The loading of CoPPc-CNT was ∼1.8 mg cm^{-2}. (b) Cycling performance of Li/Cl_2 battery using CoPPc-CNT as the positive electrode. The stable cycling behavior of the battery was recoverable after its Coulombic efficiency decayed by pairing the cycled CoPPc-CNT electrode with a fresh Li foil and new electrolyte, suggesting that the cycle life was limited by the negative electrode and not CoPPc-CNT. The loading of CoPPc-CNT was ∼1.8 mg cm^{-2}. (c) The first discharge curve and charge−discharge behavior of Li/Cl_2 battery using FePPc-CNT as the positive electrode. The resulting Li/Cl_2 battery was able to stably cycle at a capacity higher than the first discharge capacity with a higher discharge voltage (cycling capacity/first discharge capacity = 143%). The loading of FePPc-CNT was ∼1.4 mg cm^{-2}. (d) Cycling performance of Li/Cl_2 battery using FePPc-CNT as the positive electrode. The battery was cyclable at a cycling capacity ∼143% of the first discharge capacity for more than 90 cycles. The loading of FePPc-CNT was ∼1.4 mg cm^{-2}. (e) The first discharge curve and charge−discharge behavior of Na/Cl_2 battery using FePPc-CNT as the positive electrode. The resulting Na/Cl_2 battery was able to stably cycle at a capacity that was ∼3.7 times the first discharge capacity. The loading of FePPc-CNT was ∼6.0 mg cm^{-2}. (f) Cycling performance of a Na/Cl_2 battery using CoPPc-Graphite as the positive electrode. The resulting Na/Cl_2 battery was able to stably cycle at a capacity that was ∼2.3 times the first discharge capacity for more than 80 cycles. After the Coulombic efficiency began to decay, the cycled CoPPc-Graphite electrode could pair with a new Na negative electrode and fresh electrolyte and the battery cycling could be recovered. The loading of CoPPc-Graphite was ∼3.2 mg cm^{-2}. (g) The first discharge curve and charge−discharge behavior of Na/Cl_2 battery using CoPPc-Graphite as the positive electrode. The stable cycling capacity of the battery was higher than the first discharge capacity with a higher discharge

https://doi.org/10.1021/jacs.6c02353
J. Am. Chem. Soc. 2026, 148, 22673−22686

Figure 4. continued

voltage. The loading of CoPPc-Graphite was ∼3.2 mg cm^{-2}. (h) Comparison of the ratio between the cycling capacity and the first discharge capacity and positive electrode loading between CoPPc-CNT reported in this work and previous reports on Cl_2 batteries. The reference numbers were labeled next to each data point, and CoPPc-CNT demonstrated clear advantages in both categories. Inset: the Na/Cl_2 battery using CoPPc-Graphite as the positive electrode with ∼150 Wh kg^{-1} energy density calculated based on the weight of all battery's components (negative electrode, separator, electrolyte, and positive electrode). No current collector was used for this battery. The CoPPc-Graphite was pressed into a pellet and directly put onto the coin cell case as the positive electrode.

damage happened to the electrode during cycling. However, some noticeable changes such as peak shifting and the emergence of a new peak were observed. First, the main Raman peak at ∼1538 cm^{-1} (B_{1g}, displacement of the C−N−C bridge bonds in CoPPc-CNT[40]) of the pristine CoPPc-CNT displayed a blue shift to ∼1545 cm^{-1} when the battery was stopped in discharged states (1st discharge CoPPc-CNT, discharged CoPPc-CNT, Figure S17a) and to 1551 cm^{-1} when the battery was stopped in charged state (charged CoPPc-CNT, Figure S17a). It was reported that the Raman shift of these C−N−C bridge bonds was greatly affected by the metal center, the bonding geometry, and the cavity size (distance of the N-metal-N bonds), with the C−N−C bond exhibiting the highest Raman shift when it was lengthened.[40] In our CoPPc-CNT samples, the blue shift in the C−N−C Raman peak after the CoPPc-CNT was cycled in a Na/Cl_2 battery, especially after charging, was attributed to a change in the C−N−C bond length and possibly the geometry, likely caused by the formation of Co−Cl and Na−N bonds during battery charging and the formation of NaCl during battery discharging (Figure 3b,e,f,g,h,i).

Additionally, in the charged CoPPc-CNT Raman spectrum, an extra Raman peak at ∼1485 cm^{-1} was developed and then disappeared when the CoPPc-CNT was discharged (labeled with *, Figure S17a). We attributed this peak to a change in the twist angle of the CNT during battery charging, during which the CoPPc-CNT needed to accommodate all the new species that were formed (ex. Cl_2, SO_2Cl_2, eqs 2 and 4),[41] and similar structural changes in graphite electrode was also observed in previously reported Cl_2 batteries.[8] When the battery was discharged, these newly formed species were reduced (eqs 3 and 5), and the CNT relaxed back to its original state, leading to the disappearance of the peak at ∼1485 cm^{-1} (Figure S17a).

Lastly, we also compared the Raman spectra of the same CoPPc-CNT electrode before and after being stored in an argon-filled glovebox for six months (Figure S17b,c,d). Our results indicated that when the CoPPc-CNT was stopped in the discharged state (either first discharged or discharged), the Raman spectra did not show obvious changes (Figure S17b,d). However, when the CoPPc-CNT was charged, the peak at ∼1485 cm^{-1} (detected immediately after charging) had its intensity drastically weakened after six months (Figure S17c), suggesting that during the six months period, a lot of the species that were formed during charging slowly escaped/evaporated from the CoPPc-CNT material, which led to the gradual relaxation of the CNT structure to its original state.

In addition to studying the performance of CoPPc-CNT as the positive electrode in Na/Cl_2 battery, the same material was used as the positive electrode in Li/Cl_2 battery and demonstrated similar behavior in supporting the battery to have cycling capacity exceeding the first discharge capacity (Figure 4a,b). The Li/Cl_2 battery using CoPPc-CNT as the positive electrode demonstrated a first discharge voltage of ∼3.42 V_{Li} with an areal capacity of ∼1.28 mAh cm^{-2} (Figure 4a). The reaction that occurred during the first discharge was well-known from previous studies as the reduction of $SOCl_2$ in forming SO_2 and depositing S and LiCl at the positive electrode (eq 1).[2,3,8,18] During cycling, the battery was initially able to cycle at a capacity ∼100% of the first discharge capacity and gradually had it increased to ∼1.80 mAh cm^{-2}, or 1.4 times the first discharge capacity (Figure 4b). The discharge voltage during cycling also increased from ∼3.42 V_{Li} to ∼3.51 V_{Li} (Figure 4a), which was attributed to the change from $SOCl_2$ reduction during first discharge (eq 1) to Cl_2 reduction during cycling (eq 3).[1,8−11,18] The Li/Cl_2 battery using CoPPc-CNT as the positive electrode was able to cycle at a capacity ∼100% to ∼140% of the first discharge capacity for ∼80 cycles before its Coulombic efficiency began to decay (Figure 4b). After observing a decay in the Coulombic efficiency, we disassembled the battery and paired the cycled CoPPc-CNT electrode with a new piece of Li foil and added new electrolyte into the battery. The reassembled battery was able to resume its cycling at a slightly higher capacity of 2.05 mAh cm^{-2} for more than 60 cycles before its Coulombic efficiency started to slowly decay again (Figure 4b). Similar battery behavior was also observed when the loading of CoPPc-CNT at the positive electrode was increased by ∼3.7 times (first discharge capacity = 3.03 mAh cm^{-2}, stable cycling capacity = 5.26 mAh cm^{-2}, Figure S18), further verifying that such a property of cycling capacity exceeding first discharge capacity was not loading dependent but rather an intrinsic property of the CoPPc-CNT positive electrode material.

Besides CoPPc-CNT, the metal center in CoPPc could also be changed from Co to Fe to synthesize FePPc-CNT, which was able to demonstrate similar properties in cycling capacity compared to using CoPPc-CNT as the positive electrode in Li/Cl_2 battery. The Li/Cl_2 battery using FePPc-CNT as the positive electrode demonstrated a first discharge capacity of ∼0.98 mAh cm^{-2} and a stable cycling capacity of ∼1.40 mAh cm^{-2} for more than 90 cycles (Figure 4c,d). Note that unlike CoPPc-CNT positive electrode (Figure 4b), the initial Coulombic efficiency of the FePPc-CNT positive electrode was less than 100% (Figure 4d). The reason for such difference might be a change in the metal center from Co to Fe such that the interaction between LiCl and Co−N was different from that between LiCl and Fe−N, but the details warrant further studies. Likewise, the main discharge voltage of the battery increased from ∼3.44 V_{Li} during the first discharge ($SOCl_2$ reduction, eq 1) to ∼3.56 V_{Li} (Cl_2 reduction, eq 3) during cycling. These results indicated that the metal center could be varied without affecting the cycling property of the resulting Cl_2 batteries, and changing from Co to Fe would be beneficial to the overall cost of the battery, as Fe was much cheaper than Co. In addition to Li/Cl_2 battery, FePPc-CNT could also be used as the positive electrode in Na/Cl_2 battery and demonstrated a cycling capacity (∼4.74 mAh cm^{-2}) ∼370% of the first discharge capacity (∼1.28 mAh cm^{-2}, Figure 4e).

https://doi.org/10.1021/jacs.6c02353
J. Am. Chem. Soc. 2026, 148, 22673−22686

Similar to CoPPc-CNT, the main discharge voltage for FePPc-CNT in Na/Cl_2 battery also increased from ~3.41 V_{Na} during first discharge ($SOCl_2$ reduction, eq 1) to ~3.55 V_{Na} during cycling (Cl_2 reduction, eq 3, Figure 4e). A lower discharge plateau at ~3.18 V_{Na} was also observed when FePPc-CNT was used as the positive electrode in an Na/Cl_2 battery (Figure 4e), which was attributed to the reduction of SO_2Cl_2 formed from electrolyte oxidation during battery charging (eq 5).[1,2,18] Interestingly, CoPPc-CNT and FePPc-CNT exhibited different discharge voltages in the first discharge ($SOCl_2$ reduction, eq 1) and during cycling (Cl_2 reduction, eq 3) for both Na/Cl_2 and Li/Cl_2 batteries, with the difference being the most obvious during Na/Cl_2 battery first discharge (~3.41 V for FePPc-CNT and ~3.10 V for CoPPc-CNT during Na/Cl_2 battery first discharge, Figures 2d and 4a,c,e). We attributed such a difference in the discharge voltage to a difference in the catalytic effect of the metal center (Fe vs Co) on both $SOCl_2$ reduction (eq 1) and Cl_2 reduction (eq 3), with the reduction of $SOCl_2$ being much more cation-dependent than the reduction of Cl_2, as similar phenomenon was also observed in a previous study on Li/$SOCl_2$ primary battery when different metal phthalocyanines-tetraacetamide was added into the battery.[42]

In addition to CNT, we explored using fluorinated graphite after annealing in argon (Methods) as the substrate and grew CoPPc on top of it to synthesize CoPPc-Graphite. The reason that we chose to use fluorinated graphite was because we discovered that the growth of CoPPc was much easier if the graphite was functionalized, and annealing the graphite could greatly increase the capacity of the Cl_2 batteries when the material was used as the positive electrode.[1,8,18] When CoPPc-Graphite was used as the positive electrode in Na/Cl_2 battery, the resulting battery demonstrated a cycling capacity (~2.56 mAh cm^{-2}) ~231% of the first discharge (~1.11 mAh cm^{-2}, Figure 4f,g). The charge−discharge behavior showed a similar trend as in both CoPPc-CNT and FePPc-CNT, with its main discharging plateau increased to a higher voltage compared to the first discharge. These results revealed that the effect of CoPPc on the cyclability of the Cl_2 batteries was substrate independent. Interestingly, in some batteries (both Na and Li), a small yet noticeable plateau at ~2−2.5 V appeared toward the end of discharging (Figure 4c,f). We attributed this plateau to the reduction of S that was formed during the first discharge (eq 1), as similar S reduction plateaus were observed in previous studies on Li/S and Na/S batteries and S was also proven to be a good positive electrode material in $SOCl_2$-based electrolyte.[43−45] This plateau did not always appear (Figure 4e), indicating that only a portion of the S formed was electrochemically active and could be reduced. The reasons behind the formation of electrochemically active versus inactive S warrants follow-up investigations. Additionally, we varied the amount of $CoCl_2$ (one of the starting materials, Methods) to grow different amounts of CoPPc on graphite and used the resulting materials as the positive electrode in Na/Cl_2 battery. Our results indicated that the first discharge capacity of the battery decreased as more CoPPc was grown on the graphite substrate (Figure S19), attributed to a decrease in the conductivity of the CoPPc-Graphite when more CoPPc was present in the material. As a result, it was important to find the optimal amount of starting material for the synthesis to achieve the best battery performance (Methods). We believe that the identification of a substrate with even higher capacity than both CNT and graphite and growing metal-PPc on top of it to continue improving the cycling capacity of Na/Cl_2 and Li/Cl_2 batteries represents an important future research direction to further improve the energy density of Cl_2 batteries.

In addition to the positive electrode, we analyzed the sodium negative electrode after cycling in the Na/Cl_2 battery using XPS and SEM. Our results indicated that the solid electrolyte interphase (SEI) was constituted by various components, including NaCl, sodium fluoride, aluminum chloride, S, and bis(fluorosulfonyl)imide salts (Figure S20a−e). The sodium fluoride was likely formed by the decomposition of sodium bis(fluorosulfonyl)imide that was introduced in the electrolyte as an electrolyte additive. SEM imaging revealed that the SEI layer was mostly made up of square-shaped NaCl crystals, resulting from the reaction between sodium and thionyl chloride (Figure S20f). When the battery died and stopped cycling, we examined the Na negative electrode by using SEM. Our results indicated that the Na electrode was completely passivated by a thick layer of insulating NaCl, making the electrode unable to support an efficient Na plating/stripping with facile ion transport and thus leading to the eventual battery cycling decay (Figure S21). We proposed that the continuous formation/growth of these sodium chloride crystals likely resulted in the decay of the battery cycling, as the negative electrode became more and more insulating. This was the reason why after the battery decayed, replacing the negative electrode and adding new electrolyte while keeping the cycled positive electrode could recover battery cycling. As a result, finding an effective method to mitigate the continuous formation of these insulating components represents an important future research direction for further improving the cycle life of the battery.

Lastly, we compared our CoPPc-CNT material reported in this work with previous reports on Cl_2 batteries or similar battery systems in terms of the reported positive electrode loading and the ratio between the cycling capacity and the first discharge capacity.[1,8−12,18,20,46] Our CoPPc-CNT positive electrode in both Na/Cl_2 and Li/Cl_2 batteries demonstrated significant advantages in both categories when compared with other positive electrode materials used for Cl_2 batteries or for similar batteries systems (Figure 4h, Table S5). Note that the two metrics that we included in our comparison was independent of the battery cycle life, so the fact that we could improve the cycle life of the batteries by replacing the negative electrode and adding new electrolyte (Figures 2e and 4b,f) did not sacrifice the fairness in our comparison. The advantage of the cycling capacity well exceeding the first discharge capacity was the ability to use a minimal amount of electrolyte in the Cl_2 battery. Assuming everything else the same, just by lowering the electrolyte volume from 100 μL (lowest volume of electrolytes reported in previous work on Cl_2 batteries) to 50 μL (current work),[1,8,9,12,18−20] the energy density of the batteries was able to increase by ~46% in Na/Cl_2 battery and ~54% in Li/Cl_2 battery. In fact, as a proof of concept, we were able to construct a ~150 Wh kg^{-1} or ~325 Wh L^{-1} Na/Cl_2 coin cell battery using CoPPc-Graphite as the positive electrode, calculated based on the total weight of the negative electrode, separator, electrolyte, and positive electrode or the total volume of the battery, including the two electrodes and separator (Figure 4h inset). The cycle life of the ~150 Wh kg^{-1} Na/Cl_2 battery still needs further improvement, which, in our opinion, was limited by the stability of the negative electrode (Figure 2e, Figure 4f, Figures S20 and S21). Under such a high-energy-density cycling (~150 Wh kg^{-1} with higher

https://doi.org/10.1021/jacs.6c02353
J. Am. Chem. Soc. 2026, 148, 22673−22686

CoPPc-Graphite loading of ~13.4 mg cm^{-2}, Figure 4h inset), the Na negative electrode was cycling under a more challenging condition (more Na deposition/stripping per cycle at a higher current density as a result of the higher positive electrode loading), leading to the battery's current inferior cycle life. We have demonstrated that with a lower CoPPc-Graphite loading at the positive electrode (~3.2 mg cm^{-2}, Figure 4f), the resulting Na/Cl_2 battery exhibited a much-improved cycle life. Therefore, the improvement of the negative electrode's stability represents an important future research direction to further enhance the cycle life of the battery even under a high-energy-density cycling condition. Using this coin cell battery as a reference, when the battery is constructed into a pouch cell, the energy density of the entire pouch cell including packaging is projected to be at least 175 Wh kg^{-1} (assuming positive electrode area: 4 cm^2, negative electrode area: 4.41 cm^2, packaging weight = 10% of the total weight of the battery). We believe that further improvement in the batteries' energy density is possible if a new material with an even higher capacity can be identified and used as the substrate to grow metal-PPc. The final material can then be explored as the positive electrode in Cl_2 batteries.

CONCLUSION

In this work, we reported a new positive electrode material, namely CoPPc-CNT, that can support a cycling capacity well exceeding the first discharge capacity in both Na/Cl_2 and Li/Cl_2 batteries. We employed SEM to reveal that during battery discharging, CoPPc-CNT facilitated the formation of submicron-sized NaCl crystals with excellent electrochemical activity by providing nucleation points on the positive electrode surface. We also employed XPS together with theoretical calculations to reveal that during battery charging, the Co center in CoPPc bonded with Cl (Co−Cl) and the pyrrolic N in CoPPc bonded with Na (Na−N), allowing the CoPPc to act as an electrocatalyst for the reversible redox between NaCl and Cl_2. In other words, NaCl oxidation could be catalytically enhanced on the CoPPc-CNT positive electrode. Additionally, CoPPc behaved as a better Cl_2 storage medium than pure CNT, leading to improved cycling capacity when CoPPc-CNT was used as the positive electrode in Cl_2 batteries. The combination effect of CoPPc being a facilitator for the formation of submicron-sized NaCl crystals with good electrochemical activity, an electrocatalyst for reversible Cl^-/Cl_2 redox, and an excellent Cl_2 storage medium allowed the resulting Cl_2 batteries to have cycling capacity well exceeding the first discharge capacity when CoPPc-CNT was used as the positive electrode. Lastly, we could also vary the metal from Co to Fe and the CNT substrate to graphite to synthesize FePPc-CNT and CoPPc-Graphite, both of which were able to support a cycling capacity higher than the first discharge capacity in both Na/Cl_2 and Li/Cl_2 batteries. By using only a minimal amount of electrolyte, the energy density of the Cl_2 batteries can be greatly improved, and we were able to construct a prototype Na/Cl_2 coin cell battery with an energy density of ~150 Wh kg^{-1} or ~325 Wh L^{-1}. We believe that this type of material can be further explored, especially in identifying a new substrate with a higher capacity for the growth of metal-PPc. With higher capacity and excellent cyclability, the energy density of the resulting Cl_2 batteries is expected to be further improved.

ASSOCIATED CONTENT

Data Availability Statement

The data that support the findings of this study are available in the Supporting Information of this article.

Supporting Information

The Supporting Information is available free of charge at https://pubs.acs.org/doi/10.1021/jacs.6c02353.

Methods (experimental procedures) and additional figures and tables to support discussion (PDF)

AUTHOR INFORMATION

Corresponding Authors

Yang Shao-Horn − *Department of Materials Science and Engineering, Research Laboratory of Electronics, Department of Chemistry, and Department of Mechanical Engineering, Massachusetts Institute of Technology, Cambridge, Massachusetts 02139, United States;* orcid.org/0000-0001-8714-2121; Email: shaohorn@mit.edu

Ju Li − *Department of Nuclear Science and Engineering and Department of Materials Science and Engineering, Massachusetts Institute of Technology, Cambridge, Massachusetts 02139, United States;* orcid.org/0000-0002-7841-8058; Email: liju@mit.edu

Authors

Guanzhou Zhu − *Department of Nuclear Science and Engineering, Massachusetts Institute of Technology, Cambridge, Massachusetts 02139, United States*

Hongbin Xu − *Department of Materials Science and Engineering and Research Laboratory of Electronics, Massachusetts Institute of Technology, Cambridge, Massachusetts 02139, United States;* orcid.org/0009-0007-6311-475X

Shuo Wang − *Eastern Institute for Advanced Study, Eastern Institute of Technology, Ningbo, China 315200;* orcid.org/0000-0002-7907-9676

Yilin Zhang − *Eastern Institute for Advanced Study, Eastern Institute of Technology, Ningbo, China 315200*

Jen-Hung Fang − *Department of Aeronautics and Astronautics, Massachusetts Institute of Technology, Cambridge, Massachusetts 02139, United States;* orcid.org/0000-0001-8665-4088

Tao Dai − *Department of Nuclear Science and Engineering, Massachusetts Institute of Technology, Cambridge, Massachusetts 02139, United States*

Daniel J. Zheng − *Department of Materials Science and Engineering and Research Laboratory of Electronics, Massachusetts Institute of Technology, Cambridge, Massachusetts 02139, United States;* orcid.org/0000-0002-9471-6856

Weiyin Chen − *Department of Nuclear Science and Engineering, Massachusetts Institute of Technology, Cambridge, Massachusetts 02139, United States;* orcid.org/0000-0002-6427-4129

Heejung Roh − *Department of Materials Science and Engineering and Department of Chemistry, Massachusetts Institute of Technology, Cambridge, Massachusetts 02139, United States*

Daniel Wang − *Department of Mechanical Engineering, Massachusetts Institute of Technology, Cambridge, Massachusetts 02139, United States*

Davide Menga − *Research Laboratory of Electronics, Massachusetts Institute of Technology, Cambridge, Massachusetts 02139, United States*
Sunmoon Yu − *Research Laboratory of Electronics, Massachusetts Institute of Technology, Cambridge, Massachusetts 02139, United States;* orcid.org/0000-0001-7250-9365
Haldrian Iriawan − *Department of Materials Science and Engineering and Research Laboratory of Electronics, Massachusetts Institute of Technology, Cambridge, Massachusetts 02139, United States;* orcid.org/0000-0002-2997-1180

Complete contact information is available at: https://pubs.acs.org/10.1021/jacs.6c02353

Author Contributions

G.Z. and H.X. contributed equally to this work.

Notes

The authors declare no competing financial interest.

■ ACKNOWLEDGMENTS

This work was supported by MIT. Part of this work was performed in part in the MIT.nano Characterization Facilities.

■ REFERENCES

(1) Zhu, G.; Tian, X.; Tai, H.-C.; Li, Y.-Y.; Li, J.; Sun, H.; Liang, P.; Angell, M.; Huang, C.-L.; Ku, C.-S.; Hung, W.-H.; Jiang, S.-K.; Meng, Y.; Chen, H.; Lin, M.-C.; Hwang, B.-J.; Dai, H. Rechargeable Na/Cl_2 and Li/Cl_2 batteries. *Nature* **2021**, *596* (7873), 525−530.
(2) Abraham, K. M.; Mank, R. M. Some Chemistry in the Li /$SOCl_2$ Cell. *J. Electrochem. Soc.* **1980**, *127* (10), 2091.
(3) Venkatasetty, H. V.; Saathoff, D. J. Properties of $LiAlCl_4$-$SOCl_2$ Solutions for Li/$SOCl_2$ Battery. *J. Electrochem. Soc.* **1981**, *128* (4), 773.
(4) Gangadharan, R.; Namboodiri, P. N. N.; Prasad, K. V.; Viswanathan, R. The lithium—thionyl chloride battery—a review. *J. Power Sources* **1979**, *4* (1), 1−9.
(5) Behl, W. K. Electrochemical reduction of thionyl chloride in $LiAlCl_4$-$SOCl_2$ solutions. *Journal of Electroanalytical Chemistry and Interfacial Electrochemistry* **1979**, *101* (3), 367−373.
(6) Evans, T. I.; Nguyen, T. V.; White, R. E. A Mathematical Model of a Lithium/Thionyl Chloride Primary Cell. *J. Electrochem. Soc.* **1989**, *136* (2), 328.
(7) Tsaur, K. C.; Pollard, R. Mathematical Modeling of the Lithium, Thionyl Chloride Static Cell: I. Neutral Electrolyte. *J. Electrochem. Soc.* **1984**, *131* (5), 975.
(8) Zhu, G.; Liang, P.; Huang, C.-L.; Huang, C.-C.; Li, Y.-Y.; Wu, S.-C.; Li, J.; Wang, F.; Tian, X.; Huang, W.-H.; Jiang, S.-K.; Hung, W.-H.; Chen, H.; Lin, M.-C.; Hwang, B.-J.; Dai, H. High-Capacity Rechargeable Li/Cl_2 Batteries with Graphite Positive Electrodes. *J. Am. Chem. Soc.* **2022**, *144* (49), 22505−22513.
(9) Xu, Y.; Jiao, L.; Ma, J.; Zhang, P.; Tang, Y.; Liu, L.; Liu, Y.; Ding, H.; Sun, J.; Wang, M.; Li, Z.; Jiang, H.-L.; Chen, W. Metal-organic frameworks for nanoconfinement of chlorine in rechargeable lithium-chlorine batteries. *Joule* **2023**, *7* (3), 515−528.
(10) Xu, Y.; Wang, M.; Sajid, M.; Meng, Y.; Xie, Z.; Sun, L.; Jin, J.; Chen, W.; Zhang, S. Organocatalytic Lithium Chloride Oxidation by Covalent Organic Frameworks for Rechargeable Lithium-Chlorine Batteries. *Angew. Chem., Int. Ed.* **2024**, *63* (7), No. e202315931.
(11) Xu, Y.; Zhang, S.; Wang, M.; Meng, Y.; Xie, Z.; Sun, L.; Huang, C.; Chen, W. Enrichment of Chlorine in Porous Organic Nanocages for High-Performance Rechargeable Lithium−Chlorine Batteries. *J. Am. Chem. Soc.* **2023**, *145* (50), 27877−27885.
(12) Ma, C.; Feng, W.; Kong, D.; Wei, X.; Gong, X.; Yang, J.; Han, J.; Zhi, L. Vertical-Channel Cathode Host Enables Rapid Deposition Kinetics toward High-Areal-Capacity Sodium-Chlorine Batteries. *Small* **2024**, *20*, No. 2310978.
(13) Xiang, L.; Xu, Q.; Zhang, H.; Geng, S.; Cui, R.; Xiao, T.; Chen, P.; Wu, L.; Yu, W.; Peng, H.; Mai, Y.; Sun, H. Ultrahigh-Rate Na/Cl_2 Batteries Through Improved Electron and Ion Transport by Heteroatom-Doped Bicontinuous-Structured Carbon. *Angew. Chem., Int. Ed.* **2023**, *62* (47), No. e202312001.
(14) Liu, B.; Ge, Y.; Lin, C.; Jiang, H.; Qiu, T.; Li, J.; Zhang, H.; Yang, J.; Tian, X. Interlayer chemical confinement enables highly reversible and durable lithium−chlorine batteries. *Energy Environ. Sci.* **2026**, *19*, 2184.
(15) Song, Y.; Ouyang, H.; Wang, T.; Zhang, K.; Li, Z.; Li, K.; Xu, Z.; Yang, J. Unlocking Wide-Temperature Operation of High-Capacity Rechargeable Li/$SOCl_2$ Batteries with an Activated Carbon Host Featuring Catalytic Activity. *ACS Appl. Mater. Interfaces* **2026**, *18* (3), 5217−5228.
(16) Xu, Q.; Geng, S.; Yuan, B.; Liao, M.; Ye, L.; Zhao, X.; Wang, Y.; Zhang, X.; Wang, S.; Qu, Z.; Miao, H.; Yang, Z.; Gao, Y.; Wang, B.; Zhou, Y.; Peng, H.; Sun, H. A Low-Cost and Recyclable Mg/$SOCl_2$ Primary Battery Via Synergistic Solvation and Kinetics Regulation. *Adv. Funct. Mater.* **2023**, *33* (5), No. 2210343.
(17) Yuan, B.; Wu, L.; Geng, S.; Xu, Q.; Zhao, X.; Wang, Y.; Liao, M.; Ye, L.; Qu, Z.; Zhang, X.; Wang, S.; Ouyang, Z.; Tang, S.; Peng, H.; Sun, H. Unlocking Reversible Silicon Redox for High-Performing Chlorine Batteries. *Angew. Chem., Int. Ed.* **2023**, *62* (37), No. e202306789.
(18) Liang, P.; Zhu, G.; Huang, C.-L.; Li, Y.-Y.; Sun, H.; Yuan, B.; Wu, S.-C.; Li, J.; Wang, F.; Hwang, B.-J.; Dai, H. Rechargeable Li/Cl_2 Battery Down to − 80 °C. *Adv. Mater.* **2024**, *36*, No. 2307192.
(19) Zhu, G.; Liang, P.; Huang, C.-L.; Wu, S.-C.; Huang, C.-C.; Li, Y.-Y.; Jiang, S.-K.; Huang, W.-H.; Li, J.; Wang, F.; Hwang, B.-J.; Dai, H. Shedding light on rechargeable Na/Cl_2 battery. *Proc. Natl. Acad. Sci. U. S. A.* **2023**, *120* (39), No. e2310903120.
(20) Feng, W.; Wei, X.; Yang, J.; Ma, C.; Sun, Y.; Han, J.; Kong, D.; Zhi, L. Iodine-induced self-depassivation strategy to improve reversible kinetics in Na-Cl_2 battery. *Nat. Commun.* **2024**, *15* (1), 6904.
(21) Xu, Q.; Tang, S.; Li, N.; Wang, Y.; Zhao, X.; Zhang, X.; Geng, S.; Yuan, B.; Wang, S.; Ouyang, Z.; Liao, M.; Ma, L.; Shang, M.; Sun, Y.; Peng, H.; Sun, H. Harnessing organic electrolyte for non-corrosive and wide-temperature Na-Cl_2 battery. *Nat. Commun.* **2025**, *16* (1), 1946.
(22) Yuan, B.; Xu, Q.; Tang, S.; Geng, S.; Chen, Q.; Wang, Y.; Zhao, X.; Zhang, C.; Wang, S.; Ouyang, Z.; Sun, H. A wide-temperature Li/Cl_2 battery using an ester-based electrolyte. *Science China Chemistry* **2025**, *68* (9), 4408−4414.
(23) Osswald, S.; Havel, M.; Gogotsi, Y. Monitoring oxidation of multiwalled carbon nanotubes by Raman spectroscopy. *J. Raman Spectrosc.* **2007**, *38* (6), 728−736.
(24) Zdrojek, M.; Gebicki, W.; Jastrzebski, C.; Melin, T.; Huczko, A. Studies of multiwall carbon nanotubes using Raman spectroscopy and atomic force microscopy. *Solid State Phenomena* **2004**, *99*, 265−268.
(25) Han, N.; Wang, Y.; Ma, L.; Wen, J.; Li, J.; Zheng, H.; Nie, K.; Wang, X.; Zhao, F.; Li, Y.; Fan, J.; Zhong, J.; Wu, T.; Miller, D. J.; Lu, J.; Lee, S.-T.; Li, Y. Supported Cobalt Polyphthalocyanine for High-Performance Electrocatalytic CO_2 Reduction. *Chem.* **2017**, *3* (4), 652−664.
(26) Chen, J.; Zou, K.; Ding, P.; Deng, J.; Zha, C.; Hu, Y.; Zhao, X.; Wu, J.; Fan, J.; Li, Y. Conjugated Cobalt Polyphthalocyanine as the Elastic and Reprocessable Catalyst for Flexible Li−CO_2 Batteries. *Adv. Mater.* **2019**, *31* (2), No. 1805484.
(27) Xia, Y.; Kashtanov, S.; Yu, P.; Chang, L.-Y.; Feng, K.; Zhong, J.; Guo, J.; Sun, X. Identification of dual-active sites in cobalt phthalocyanine for electrochemical carbon dioxide reduction. *Nano Energy* **2020**, *67*, No. 104163.
(28) Shchukarev, A.; Boily, J.-F. XPS study of the hematite−aqueous solution interface. *Surf. Interface Anal.* **2008**, *40* (3−4), 349−353.

(29) Kohiki, S.; Ohmura, T.; Kusao, K. Appraisal of a new charge correction method in x-ray photoelectron spectroscopy. *J. Electron Spectrosc. Relat. Phenom.* **1983**, *31* (1), 85−90.
(30) Nefedov, V. I.; Salyn, Y. V.; Leonhardt, G.; Scheibe, R. A comparison of different spectrometers and charge corrections used in X-ray photoelectron spectroscopy. *J. Electron Spectrosc. Relat. Phenom.* **1977**, *10* (2), 121−124.
(31) Kai, S.; Ulrik, G.; Hans, S.; Erik, O. Angular Distribution of Electrons in ESCA Spectra from a Single Crystal. *Phys. Scr.* **1970**, *1* (5−6), 272.
(32) Li, C.; Patra, J.; Li, J.; Rath, P. C.; Lin, M.-H.; Chang, J.-K. A Novel Moisture-Insensitive and Low-Corrosivity Ionic Liquid Electrolyte for Rechargeable Aluminum Batteries. *Adv. Funct. Mater.* **2020**, *30* (12), No. 1909565.
(33) Azmi, R.; Lindgren, F.; Stokes-Rodriguez, K.; Buga, M.; Ungureanu, C.; Gouveia, T.; Christensen, I.; Pal, S.; Vlad, A.; Ladam, A.; Edström, K.; Hahlin, M. An XPS Study of Electrolytes for Li-Ion Batteries in Full Cell LNMO vs Si/Graphite. *ACS Appl. Mater. Interfaces* **2024**, *16* (26), 34266−34280.
(34) Schweigart, P.; Eleri, O. E.; Nylund, I.-E.; Lai, S. Y.; Lou, F.; Svensson, A. M. On the Viability of Lithium Bis(fluorosulfonyl)imide as Electrolyte Salt for Use in Lithium-Ion Capacitors. *Batteries & Supercaps* **2023**, *6* (9), No. e202300226.
(35) Klinedinst, K. A.; McLaughlin, M. L. Solubilities of sulfur and sulfur dioxide in thionyl chloride with and without 1.8 M lithium tetrachloroaluminate. *Journal of Chemical & Engineering Data* **1979**, *24* (3), 203−206.
(36) Hammer, B.; Hansen, L. B.; Nørskov, J. K. Improved adsorption energetics within density-functional theory using revised Perdew-Burke-Ernzerhof functionals. *Phys. Rev. B* **1999**, *59* (11), 7413−7421.
(37) Wellendorff, J.; Lundgaard, K. T.; Møgelhøj, A.; Petzold, V.; Landis, D. D.; Nørskov, J. K.; Bligaard, T.; Jacobsen, K. W. Density functionals for surface science: Exchange-correlation model development with Bayesian error estimation. *Phys. Rev. B* **2012**, *85* (23), No. 235149.
(38) Furness, J. W.; Kaplan, A. D.; Ning, J.; Perdew, J. P.; Sun, J. Accurate and Numerically Efficient r2SCAN Meta-Generalized Gradient Approximation. *J. Phys. Chem. Lett.* **2020**, *11* (19), 8208−8215.
(39) Ning, J.; Kothakonda, M.; Furness, J. W.; Kaplan, A. D.; Ehlert, S.; Brandenburg, J. G.; Perdew, J. P.; Sun, J. Workhorse minimally empirical dispersion-corrected density functional with tests for weakly bound systems: r^{2}SCAN + rVV10. *Phys. Rev. B* **2022**, *106* (7), No. 075422.
(40) Tackley, D. R.; Dent, G.; Ewen Smith, W. Phthalocyanines: structure and vibrations. *Phys. Chem. Chem. Phys.* **2001**, *3* (8), 1419−1426.
(41) Uhm, T.; Na, J.; Lee, J.-U.; Cheong, H.; Lee, S. W.; Campbell, E. E. B.; Jhang, S. H. Structural configurations and Raman spectra of carbon nanoscrolls. *Nanotechnology* **2020**, *31* (31), No. 315707.
(42) Xu, Z.; Li, K.; Wang, R.; Duan, X.; Liu, Q.; Zhang, R.; Zhao, J. Electrochemical Effects of Lithium-Thionyl Chloride Battery by Central Metal Ions of Phthalocyanines-Tetraacetamide Complexes. *J. Electrochem. Soc.* **2017**, *164* (14), No. A3628.
(43) Su, Y.-S.; Fu, Y.; Cochell, T.; Manthiram, A. A strategic approach to recharging lithium-sulphur batteries for long cycle life. *Nat. Commun.* **2013**, *4* (1), 2985.
(44) Yu, X.; Manthiram, A. Capacity Enhancement and Discharge Mechanisms of Room-Temperature Sodium−Sulfur Batteries. *ChemElectroChem.* **2014**, *1* (8), 1275−1280.
(45) Geng, S.; Yuan, B.; Zhao, X.; Xu, Q.; Wang, Y.; Ouyang, Z.; Tang, S.; Wang, S.; Zhang, C.; Chen, Q.; Liao, M.; Wang, B.; Zhao, C.; Jin, W.; Li, Z.; Ye, T.-N.; Gong, X.; Peng, H.; Sun, H. High-voltage anode-free sodium−sulfur batteries. *Nature* **2026**, *649* (8096), 353−359.
(46) Xia, M.; Feng, Y.; Wei, J.; Rao, A. M.; Zhou, J.; Lu, B. A Rechargeable K/Br Battery. *Adv. Funct. Mater.* **2022**, *32* (38), No. 2205879.

https://doi.org/10.1021/jacs.6c02353
J. Am. Chem. Soc. 2026, 148, 22673−22686

Supplementary Information

Increasingly Reversible Na/Cl_2 and Li/Cl_2 Batteries

Guanzhou Zhu[1,&], Hongbin Xu[2,3,&], Shuo Wang[4], Yilin Zhang[4], Jen-Hung Fang[5], Tao Dai[1], Daniel J. Zheng[2,3], Weiyin Chen[1], Heejung Roh[2,6], Daniel Wang[7], Davide Menga[3], Sunmoon Yu[3], Haldrian Iriawan[2,3], Yang Shao-Horn[2,3,6,7,*], Ju Li[1,2,*]

[1]Department of Nuclear Science and Engineering, Massachusetts Institute of Technology, Cambridge, Massachusetts 02139, USA.
[2]Department of Materials Science and Engineering, Massachusetts Institute of Technology, Cambridge, Massachusetts 02139, USA.
[3]Research Laboratory of Electronics, Massachusetts Institute of Technology, Cambridge, Massachusetts 02139, USA.
[4]Eastern Institute for Advanced Study, Eastern Institute of Technology, Ningbo, China, 315200.
[5]Department of Aeronautics and Astronautics, Massachusetts Institute of Technology, Massachusetts 02139, USA.
[6]Department of Chemistry, Massachusetts Institute of Technology, Cambridge, Massachusetts 02139, USA.
[7]Department of Mechanical Engineering, Massachusetts Institute of Technology, Cambridge, Massachusetts 02139, USA.
[&]These authors contributed equally to this work.
*Corresponding author. Emails: shaohorn@mit.edu (Yang Shao-Horn); liju@mit.edu (Ju Li).

Methods

Synthesis of CoPPc-CNT, FePPc-CNT, and CoPPc-Graphite

All chemicals were used as received without further purification. Milli-Q deionized water was used in all experiments. Typically, to synthesize CoPPc-CNT, 60 mg of CNT was dispersed in 30 ml of ethanol and sonicated for over 30 min. Then 36 mg of anhydrous cobalt (II) chloride ($CoCl_2$), 100 mg of 1,2,4,5-Tetracyanobenzene, and 97 mg of 4-Nitrophthalonitrile were dissolved in 30 ml ethanol with over 30 min sonication as well. After that, these two mixtures were transferred into a Teflon reactor and 86 µl of 1,8-diazabicyclo[5.4.0]undec-7-ene was added. The autoclave was placed under 180 °C for 8 h. The final product was centrifuged and washed by ethanol for three times and dried in 80 °C oven overnight. To synthesize FePPc-CNT, we simply changed the above $CoCl_2$ to iron (II) chloride ($FeCl_2$) and kept everything else the same. To synthesize CoPPc-graphite, we kept other chemicals the same but only changed CNTs to annealed fluorinated graphite. Prior to synthesizing the CoPPc-Graphite, the fluorinated graphite (American Elements, GR-FPOLY-01-P.SPEC1) was annealed in an argon environment for 1000 ^{o}C for 45 minutes inside a tube furnace (flow rate of argon = 200 sccm). Additionally, the amount of carbon substrate and Co or Fe precursors could be adjusted to have the best ratio for batteries.

Electrodes fabrication

All positive electrodes (CoPPc-CNT, FePPc-CNT, CoPPc-Graphite) were fabricated following the same protocol. As an example, after CoPPc-CNT was synthesized, it was sonicated in ethanol for 2 hours. Nickel (Ni) foam was cut into a circular shape with a diameter of 10 mm using a disc cutter (MTI, MSK-T-10). The Ni foam was sonicated in ethanol for 15 minutes and then dried in 100 ^{o}C vacuum oven until all ethanol was evaporated. The Ni foam was then weighed and clamped using a crossover tweezer and placed on a hot plate with a temperature of 110 ^{o}C. The CoPPc-CNT ink was then slowly dropped onto the Ni foam (20 µL each time) until a satisfactory loading was reached (weight of CoPPc-CNT on Ni foam minus the weight of bare Ni foam). The CoPPc-CNT on Ni foam electrodes were then stored in a 100 ^{o}C vacuum oven.

To fabricate Na negative electrode, Na metal block (Sigma-Aldrich) was taken out from mineral oil and wiped using kimwipes (Kimtech). A razor blade was used to cut all six sides of the metal block to expose the shiny Na metal. The Na metal block was then cut into smaller pieces and placed in between a piece of monolayer microporous membrane (PP, Celgard). The Na metal block was then rolled using a manual die cutting & embossing machine (Amazon) to obtain a Na foil. The Na foil was then punched using a 12 mm in diameter puncher to obtain the Na negative electrode. The Na negative electrode was then pasted onto a spacer and ready to be used.

To fabricate Li negative electrode, Li chips (MTI, EQ-Lib-LiC) were directly used. Both sides of the Li chip were scraped using a nail file to remove the surface oxide/contamination. The scraped Li chip was pasted onto a spacer and ready to be used.

Fabrication of electrolyte

The electrolyte was fabricated inside an argon-filled glovebox. To prepare the electrolyte for Na/Cl_2 battery, 4 M $AlCl_3$ (Sigma-Aldrich) and 0.07 M NaFSI (Solvionic) were dissolved in $SOCl_2$ (Spectrum Chemical MFG Corp) inside a 20 mL scintillation vial (Fisher Scientific). After both chemicals were dissolved, 3.93 M NaCl (Sigma-Aldrich) was added to the solution to neutralize the electrolyte. Normally, a slight excess of NaCl was added to ensure the neutralization of the electrolyte. The electrolyte was ready to be used after stirring for ~ 1 hour. Prior to adding the electrolyte into a battery, the electrolyte was allowed to rest (without stirring) so that the excess NaCl would fall to the bottom of the vial, and the upper clear liquid was used as the electrolyte.
To fabricate the electrolyte for Li/Cl_2 battery, similar procedures were taken, but the composition of the electrolyte was changed to 3 M $AlCl_3$, 2.95 M LiCl, and 0.05 M LiFSI in $SOCl_2$.

Batteries assembly

All batteries were assembled inside an argon-filled glovebox. After the electrolyte was fabricated, the positive electrode was transferred inside the glovebox and placed in the center of a SS316 coin cell positive electrode case. Then 37.5 μL of electrolyte was dropped on the electrode. A piece of 16 mm in diameter glass fiber separator (Whatman, GF/D) or a piece of quartz separator (Sterlitech, QR100) was placed on top of the electrode and another 37.5 μL of electrolyte was added to the separator (total electrolyte volume = 75 μL). If the total electrolyte volume added was 50 μL, then 25 μL of electrolyte was added into the battery each time. Either Na or Li negative electrode was placed directly facing the positive electrode, and a piece of spring was placed on top of the spacer. Lastly, the coin cell negative electrode case was placed to cover the whole stack, and the coin cell was sealed using a manual hydraulic crimper (MSE Supplies). After sealing, the coin cell was taken out of the glovebox and ready to be tested using a battery tester (Landt). All electrochemical tests were done at room temperature.

Raman spectroscopy measurement

Raman spectra were measured using a LabRAM HR microscope Raman spectrometer system (Horiba). The laser source used for the measurement was 633 nm. To conduct the measurement, the Raman instrument was first calibrated using a silicon wafer with its Raman peak calibrated to 520.7 cm^{-1}. After calibration, the samples were put underneath the microscope and the focus was adjusted before the Raman spectrum was collected.

Scanning electron microscopy measurement

SEM measurements were performed using a Zeiss Merlin High-resolution SEM. After the batteries were stopped in the designated state, the batteries were disassembled inside an argon-filled glovebox. The positive electrode was taken out and sealed inside an aluminum laminated pouch (MTI, T-EQ-alf-480-7.5M) in the glovebox. The electrode was then taken to the SEM instrument and transferred into the instrument. A 5.00 kV voltage was used for the measurements.

X-ray photoelectron spectroscopy

XPS measurements were performed using a Thermo Scientific K-Alpha+ XPS instrument. The sample preparation for XPS was the same as that for SEM. After the samples were transferred inside the XPS instrument, measurements of the desired elements were taken.

Theoretical calculations

The spin-polarized density functional theory (DFT) calculation is performed employing the Vienna Ab-initio Simulation Package (VASP)[1], with the projected augmented wave (PAW) method[2]. For the exchange-correlation functional, we use Perdew-Burke-Ernzerhof (PBE) of the generalized gradient approximation (GGA)[3]. The plane-wave basis energy cutoff is set to 550 eV to ensure sufficient basis set convergence. For the sampling of the Brillouin zone, the Gamma-only k-point mesh was utilized. All molecular structures underwent full geometry optimization, with the energy convergence criterion set to 10^{-7} eV and the force convergence criterion set to 10^{-3} eV $Å^{-1}$. An empirical correction (DFT-D3) was used to describe the van der Waals interaction[4].

The reaction free energy of a reaction step generating species B from species A was calculated as

$$\Delta G_{A\to B} = \Delta E_{A\to B} + \Delta ZPE_{A\to B} - T\Delta S$$

$\Delta G_{A\to B}$, $\Delta E_{A\to B}$, $\Delta ZPE_{A\to B}$ and ΔS are the difference of the calculated total energy, zero-point energy, and entropy, respectively, between reactant A and product B. The zero-point energy and entropy were estimated from vibrational frequency calculations of adsorbed intermediates. Vibrational excitation energy was neglected. In this study, T was set to the room temperature 300 K.

Three-electrode cyclic voltammetry (CV) to study Cl_2 evolution

The three-electrode CV measurements were performed using either CoPPc-CNT or CNT loaded on carbon fiber paper as the working electrode, platinum foil as the counter electrode, and reversible hydrogen electrode as the reference electrode. The electrolyte that we used was either 0.05 M sulfuric acid (H_2SO_4) and 0.10 M sodium chloride (NaCl) in deionized water (for chlorine evolution reaction) or 0.05 M H_2SO_4 and 0.10 M sodium perchlorate ($NaClO_4$) in deionized water (for oxygen evolution reaction). The scan rate was 50 mV s^{-1}. The CV was measured using a Biologic SP-200 potentiostat. To analyze the Tafel slope of chlorine evolution, the current was first averaged between the forward and backward scans to correct for capacitive currents. Then the capacitance-corrected current measured in 0.05 M H_2SO_4 + 0.10 M $NaClO_4$ was subtracted from the capacitance-corrected current measured in 0.05 M H_2SO_4 + 0.10 M NaCl to isolate the chlorine evolution reaction current. A linear line fitted to log(current) vs. potential to calculate the Tafel slope. All electrochemical tests were done at room temperature.

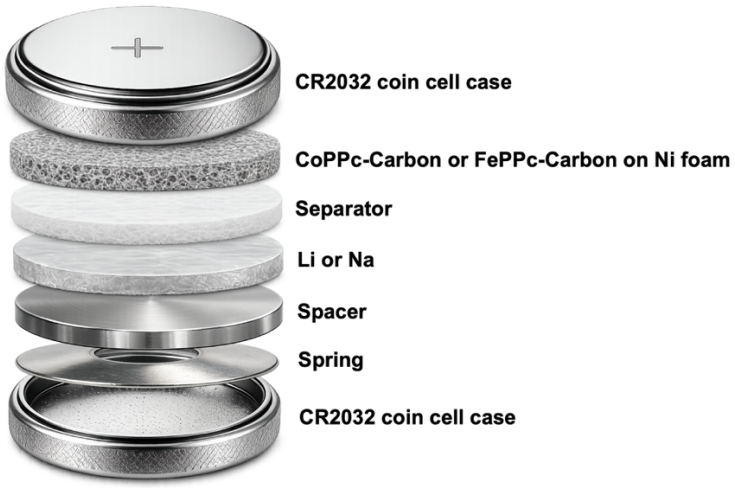

Figure S1. Schematic drawing of coin cell assembly. See Methods for more details.

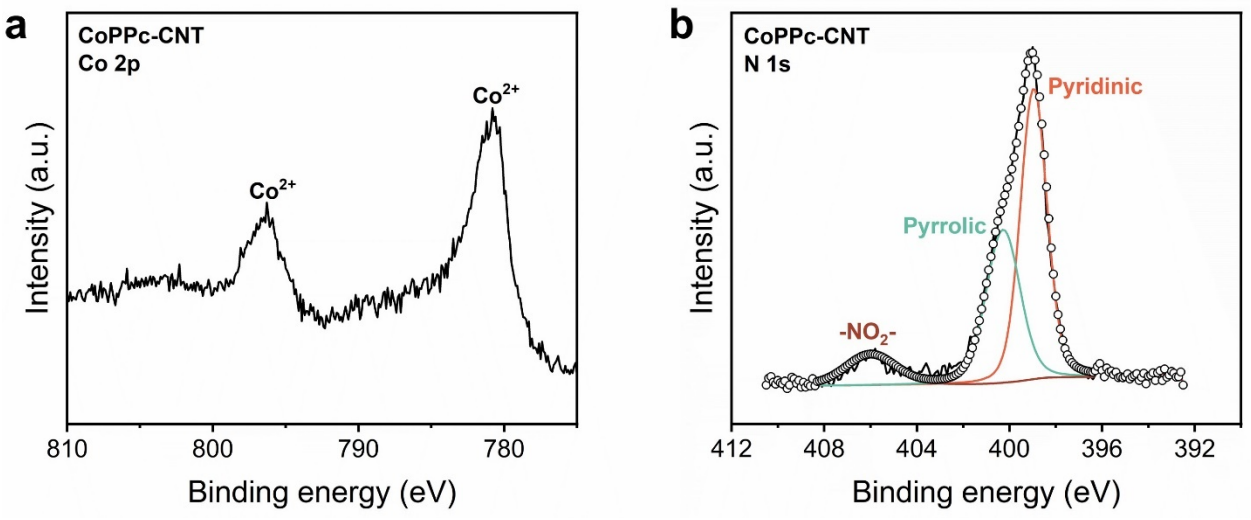

Figure S2. XPS spectra of CoPPc-CNT. a, Co 2p spectrum of CoPPc-CNT. A strong Co $2p_{3/2}$ peak at ~ 780.8 eV, corresponding to Co^{2+} in CoPPc, was observed. **b,** N 1s spectrum of CoPPc-CNT. Three distinct peaks were observed, corresponding to pyridinic N (~ 399 eV), pyrrolic N (~ 400.2 eV), and -NO_2- group (~ 406 eV) in CoPPc-CNT. The XPS spectra were calibrated by C 1s = 284.8 eV.

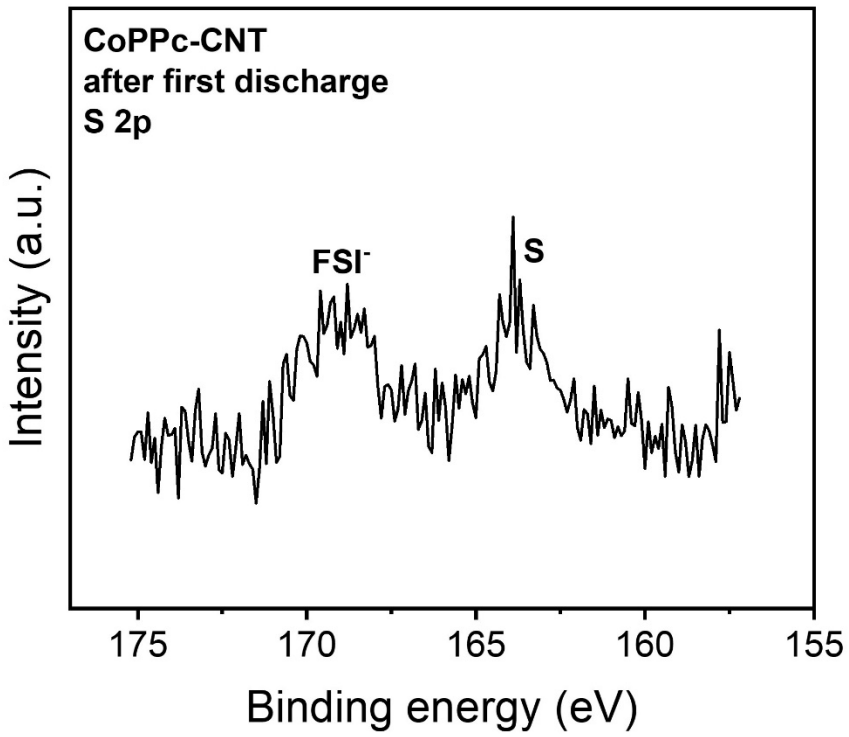

Figure S3. S 2p XPS spectrum of CoPPc-CNT electrode after the first discharge in Na/Cl_2 battery. S (formed from $SOCl_2$ reduction, eq. 1 of the main manuscript) and FSI^- (residual electrolyte) were detected.

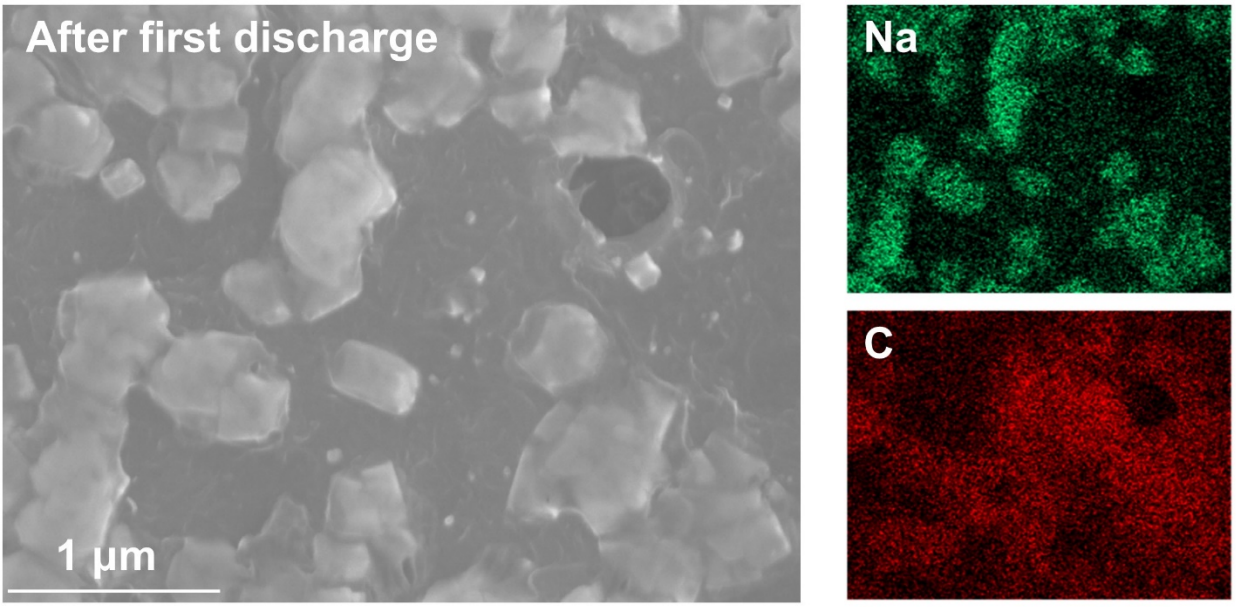

Figure S4. SEM/EDS results of the CoPPc-CNT electrode after Na/Cl_2 battery first discharge. The non-overlapping signals of Na and C indicated that underneath the NaCl crystals was the CoPPc-CNT.

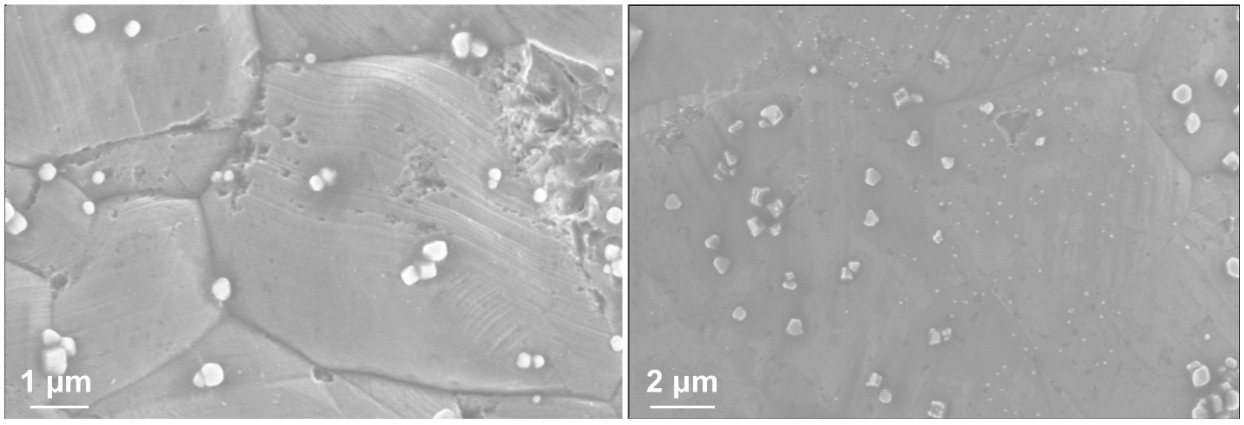

Figure S5. SEM images of the CNT positive electrode after first discharge in Na/Cl_2 battery. The NaCl crystals formed on CNT were much larger in size (tens of microns) when compared to the NaCl formed on CoPPc-CNT.

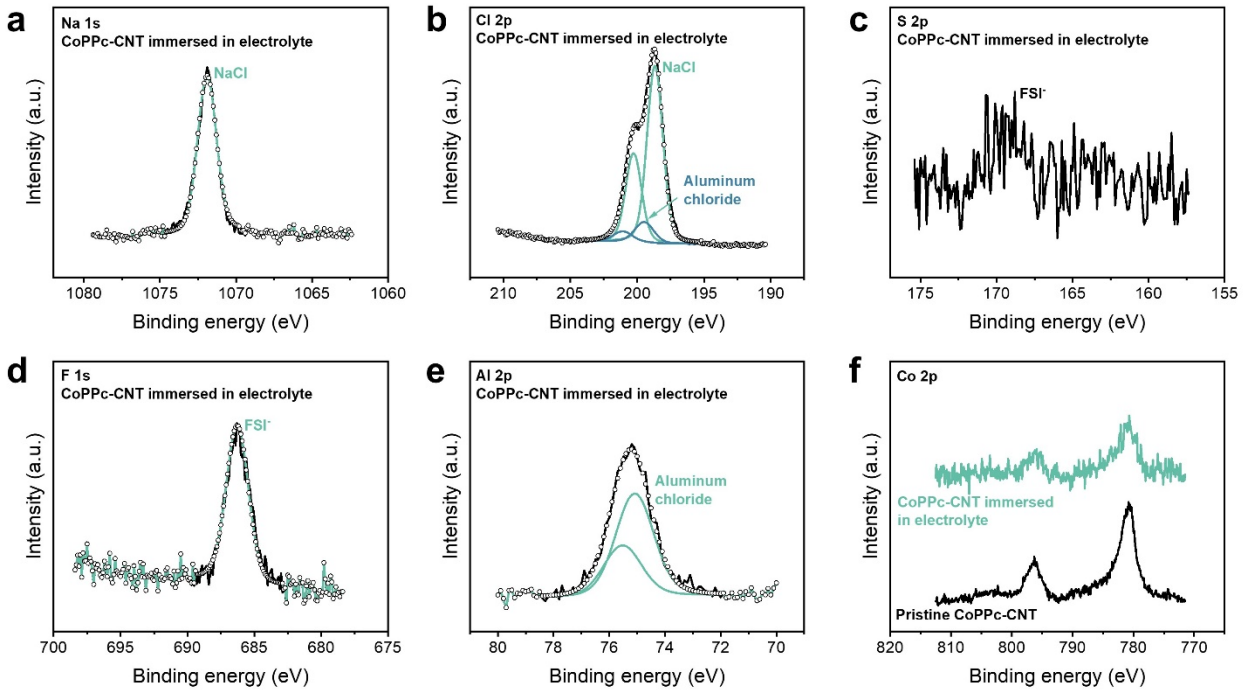

Fig. S6. XPS studies of the CoPPc-CNT electrode after immersing in Na battery electrolyte. **a,** Na 1s spectrum. **b,** Cl 2p spectrum. **c,** S 2p spectrum. **d,** F 1s spectrum. **e,** Al 2p spectrum. **f,** Co 2p spectrum. The XPS results indicated that NaCl, FSI^-, and aluminum chloride were present on the electrode, and CoPPc did not undergo obvious changes before and after immersing in the electrolyte.

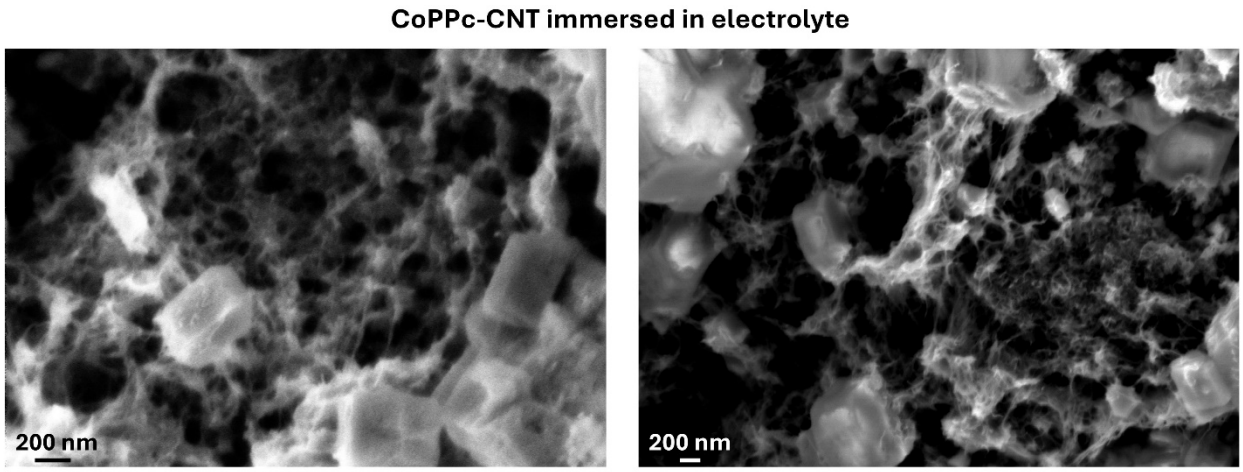

Figure S7. SEM images of CoPPc-CNT electrode after immersing in Na battery electrolyte. Sparse NaCl crystals were present at the electrode surface.

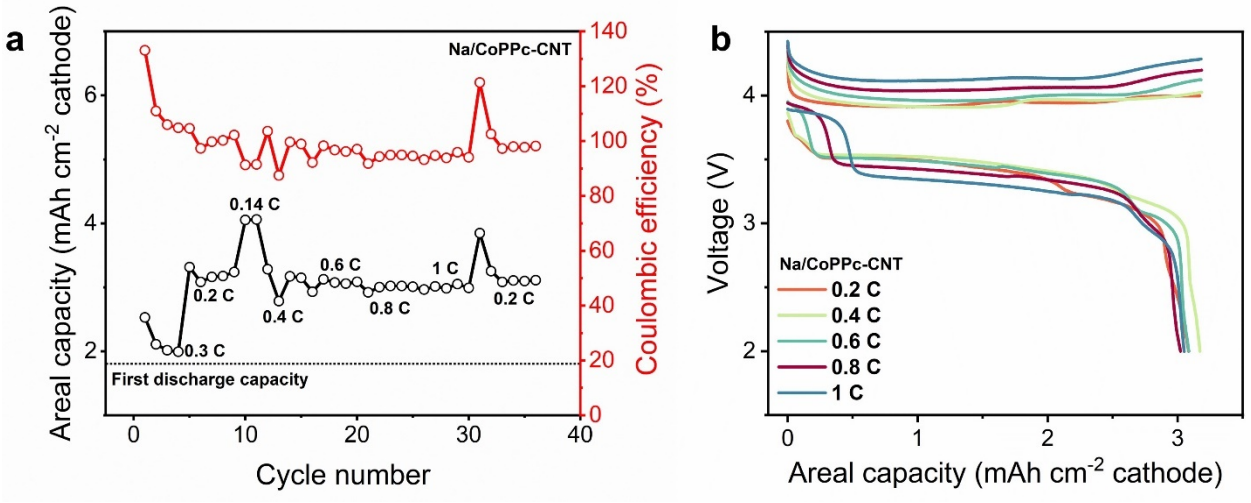

Figure S8. Rate studies of Na/Cl_2 battery using CoPPc-CNT as the positive electrode. a, Cycling performance of the battery at various rates (0.2 C to 1 C). **b,** Charge-discharge curves of the battery at various rates (0.2 C to 1 C). The battery could stably cycle at up to 1 C rate with an areal capacity of ~ 3 mAh cm^{-2}. The loading of CoPPc-CNT was ~ 3.2 mg cm^{-2}.

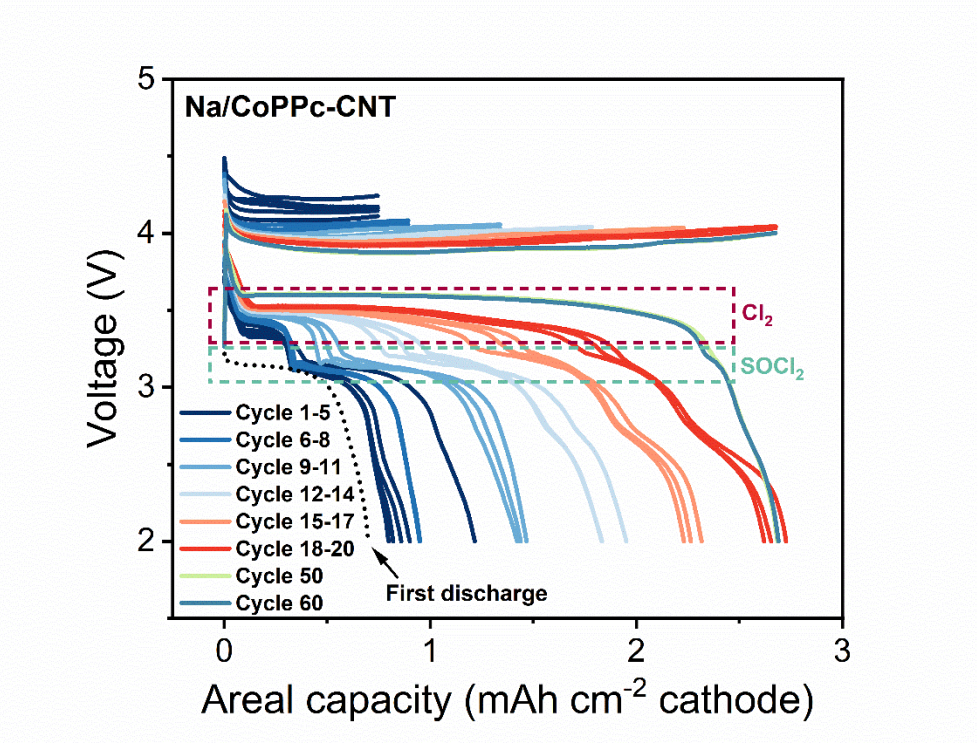

Figure S9. The first discharge, first 20 cycles, and the 50th and 60th cycles of charge-discharge curves of Na/Cl_2 battery using CoPPc-CNT as the positive electrode. The first discharge (black dotted curve) exhibited a discharging voltage of ~ 3.1 V_{Na}, corresponding to the reduction of $SOCl_2$. A higher discharging plateau in the range of 3.4 V_{Na}-3.6 V_{Na} appeared during battery charge-discharge, corresponding to the reduction of Cl_2.

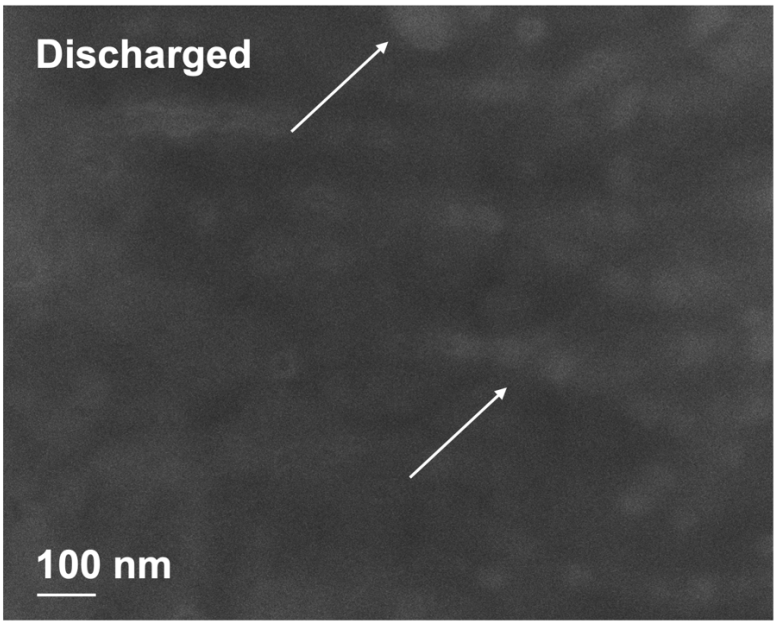

Figure S10. SEM image of discharged CoPPc-CNT electrode in Na/Cl_2 battery at the same magnification as Fig. 3a of the main text. Due to the more insulating nature of the discharged CoPPc-CNT electrode, at such a high magnification, the submicron-sized NaCl crystals on the electrode could not be as easily seen (indicated by white arrows).

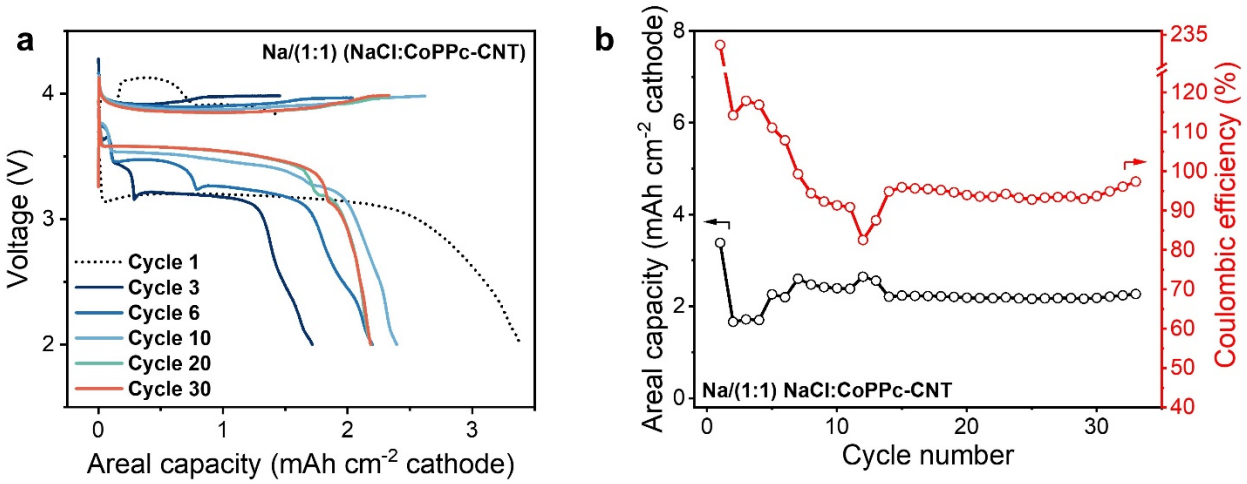

Figure S11. The charge-discharge curves and cycling performance of Na/Cl_2 battery using pre-deposited NaCl in CoPPc-CNT as the positive electrode. a, Charge-discharge curves of Na/Cl_2 battery using pre-deposited NaCl in CoPPc-CNT as the positive electrode. **b,** Cycling performance of Na/Cl_2 battery using pre-deposited NaCl in CoPPc-CNT as the positive electrode.

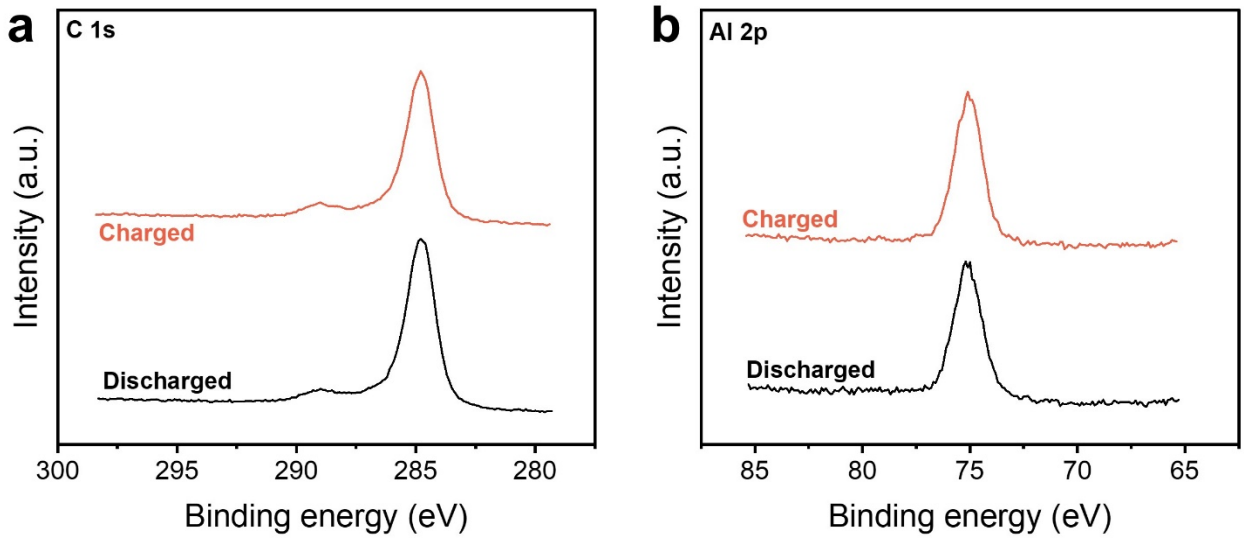

Figure S12. C 1s and Al 2p XPS spectra of charged and discharged CoPPc-CNT electrodes. **a,** C 1s XPS spectra of charged and discharged CoPPc-CNT electrodes. **b,** Al 2p XPS spectra of charged and discharged CoPPc-CNT electrodes. The XPS spectra were calibrated by C 1s = 284.8 eV.

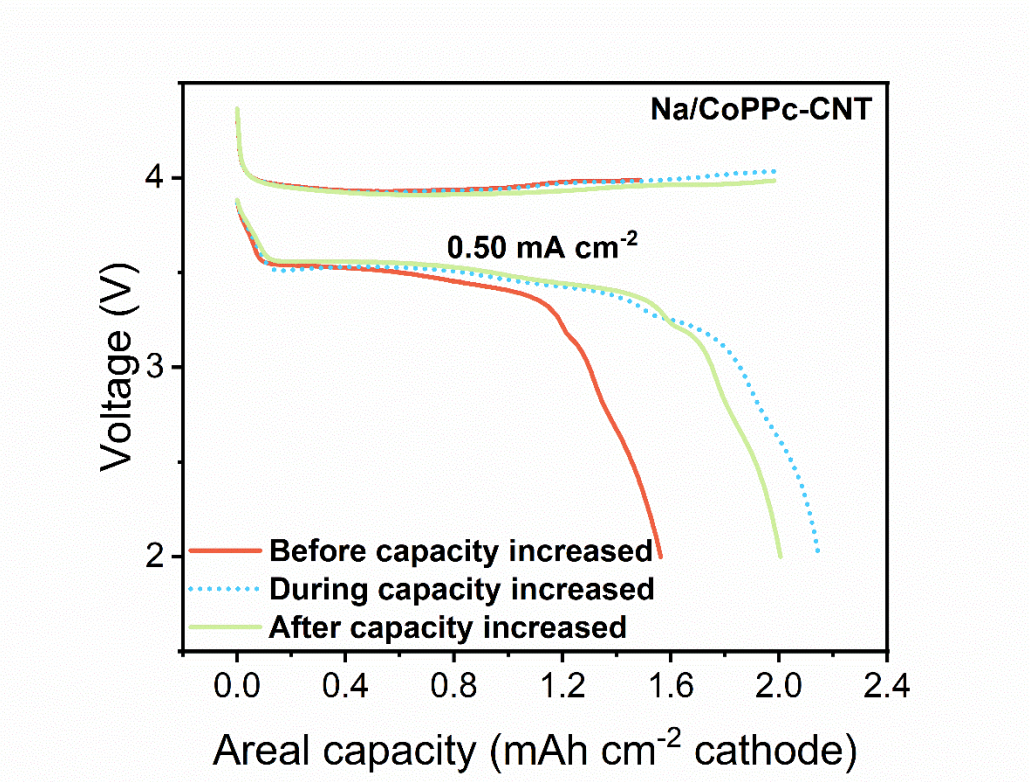

Figure S13. Charge-discharge curves comparison of Na/Cl_2 battery using CoPPc-CNT as the positive electrode at three consecutive cycles. Red solid curve: the charge-discharge cycle before the cycling capacity of the battery was increased. Blue dotted curve: the charge-discharge cycle in which the cycling capacity of the battery was increased (the cycle right after the red solid curve). Green solid curve: the charge-discharge cycle after the cycling capacity of the battery was increased (the cycle right after the blue dotted curve).

	Cl_2-Graphene	**NaCl-Graphene**	**LiCl-Graphene**	**Na-Cl**	**Li-Cl**
DFT Energy	-911.294	-912.611	-913.394	-4.677	-5.436
TΔS+ZPE	-0.126	-0.122	-0.078901	-0.057774	-0.036075
Gibbs Energy	-911.421	-912.733	-913.472	-4.735	-5.472
	Cl_2-CoPPc	**NaCl-CoPPc**	**LiCl-CoPPc**	**Cl-Graphene**	**Cl-CoPPc**
DFT Energy	-441.821	-443.549	-444.229	-908.898	-440.340
TΔS+ZPE	-0.118439	-0.107876	-0.036368	-0.090037	-0.029647
Gibbs Energy	-441.939	-443.657	-444.266	-908.988	-440.369
	Cl_2	**Cl atom**	**Na atom**	**Li atom**	**Graphene**
DFT Energy	-3.5984	-1.799	-1.469	-2.006	-907.491
TΔS+ZPE	-0.042685				
Gibbs Energy	-3.6411				
	CoPPc	**NaCl bulk**	**LiCl Bulk**		
DFT Energy	-437.745	-7.182	-7.719		

Table S1. The calculated DFT energies, ZPE + TΔS corrections and Gibbs energies of all structures in the proposed reaction pathway under PBE level. Unit is in eV.

	Cl_2-Graphene	**NaCl-Graphene**	**LiCl-Graphene**	**Na-Cl**	**Li-Cl**
DFT Energy	-875.852	-877.259	-878.006	-4.544	-5.294
TΔS+ZPE	-0.126	-0.122	-0.078	-0.057	-0.036
Gibbs Energy	-875.979	-877.381	-878.085	-4.602	-5.331
	Cl_2-CoPPc	**NaCl-CoPPc**	**LiCl-CoPPc**	**Cl-Graphene**	**Cl-CoPPc**
DFT Energy	-428.258	-430.067	-430.757	-873.713	-426.932
TΔS+ZPE	-0.118	-0.107	-0.036	-0.090	-0.029
Gibbs Energy	-428.376	-430.175	-430.793	-873.803	-426.962
	Cl_2	**Cl atom**	**Na atom**	**Li atom**	**Graphene**
DFT Energy	-3.413	-1.706	-1.454	-1.977	-872.250
TΔS+ZPE	-0.042				
Gibbs Energy	-3.456				
	CoPPc	**NaCl bulk**	**LiCl Bulk**		
DFT Energy	-424.482	-7.159	-7.618		

Table S2. The calculated DFT energies, ZPE + TΔS corrections and Gibbs energies of all structures in the proposed reaction pathway under RPBE level. Unit is in eV.

	Cl_2-Graphene	**NaCl-Graphene**	**LiCl-Graphene**	**Na-Cl**	**Li-Cl**
DFT Energy	-843.382	-844.240	-846.202	-1.231	-3.145
TΔS+ZPE	-0.126	-0.122	-0.078	-0.057	-0.036
Gibbs Energy	-843.508	-844.362	-846.281	-1.289	-3.1811
	Cl_2-CoPPc	**NaCl-CoPPc**	**LiCl-CoPPc**	**Cl-Graphene**	**Cl-CoPPc**
DFT Energy	-399.733	-401.041	-402.878	-842.454	-399.722
TΔS+ZPE	-0.118	-0.107	-0.036	-0.090	-0.029
Gibbs Energy	-399.852	-401.148	-402.914	-842.544	-399.752
	Cl_2	**Cl atom**	**Na atom**	**Li atom**	**Graphene**
DFT Energy	-0.580	-0.290	0.377	-1.358	-842.492
TΔS+ZPE	-0.042				
Gibbs Energy	-0.623				
	CoPPc	**NaCl bulk**	**LiCl Bulk**		
DFT Energy	-398.414	-3.783	-5.631		

Table S3. The calculated DFT energies, ZPE + TΔS corrections and Gibbs energies of all structures in the proposed reaction pathway under BEEF-vdW level. Unit is in eV.

	Cl_2-Graphene	**NaCl-Graphene**	**LiCl-Graphene**	**Na-Cl**	**Li-Cl**
DFT Energy	-971.83	-971.359	-970.579	-10.783	-9.961
TΔS+ZPE	-0.126	-0.122	-0.078	-0.057	-0.036
Gibbs Energy	-971.960	-971.482	-970.658	-10.841	-9.997
	Cl_2-CoPPc	**NaCl-CoPPc**	**LiCl-CoPPc**	**Cl-Graphene**	**Cl-CoPPc**
DFT Energy	-479.081	-479.104	-478.197	-965.581	-473.697
TΔS+ZPE	-0.118	-0.107	-0.036	-0.090	-0.029
Gibbs Energy	-479.200	-479.212	-478.233	-965.671	-473.726
	Cl_2	**Cl atom**	**Na atom**	**Li atom**	**Graphene**
DFT Energy	-11.497	-5.748	-3.278	-2.287	-960.131
TΔS+ZPE	-0.042				
Gibbs Energy	-11.540				
	CoPPc	**NaCl bulk**	**LiCl Bulk**		
DFT Energy	-467.177	-13.308	-12.319		

Table S4. The calculated DFT energies, ZPE + TΔS corrections and Gibbs energies of all structures in the proposed reaction pathway under r^2SCAN+RVV10 level. Unit is in eV.

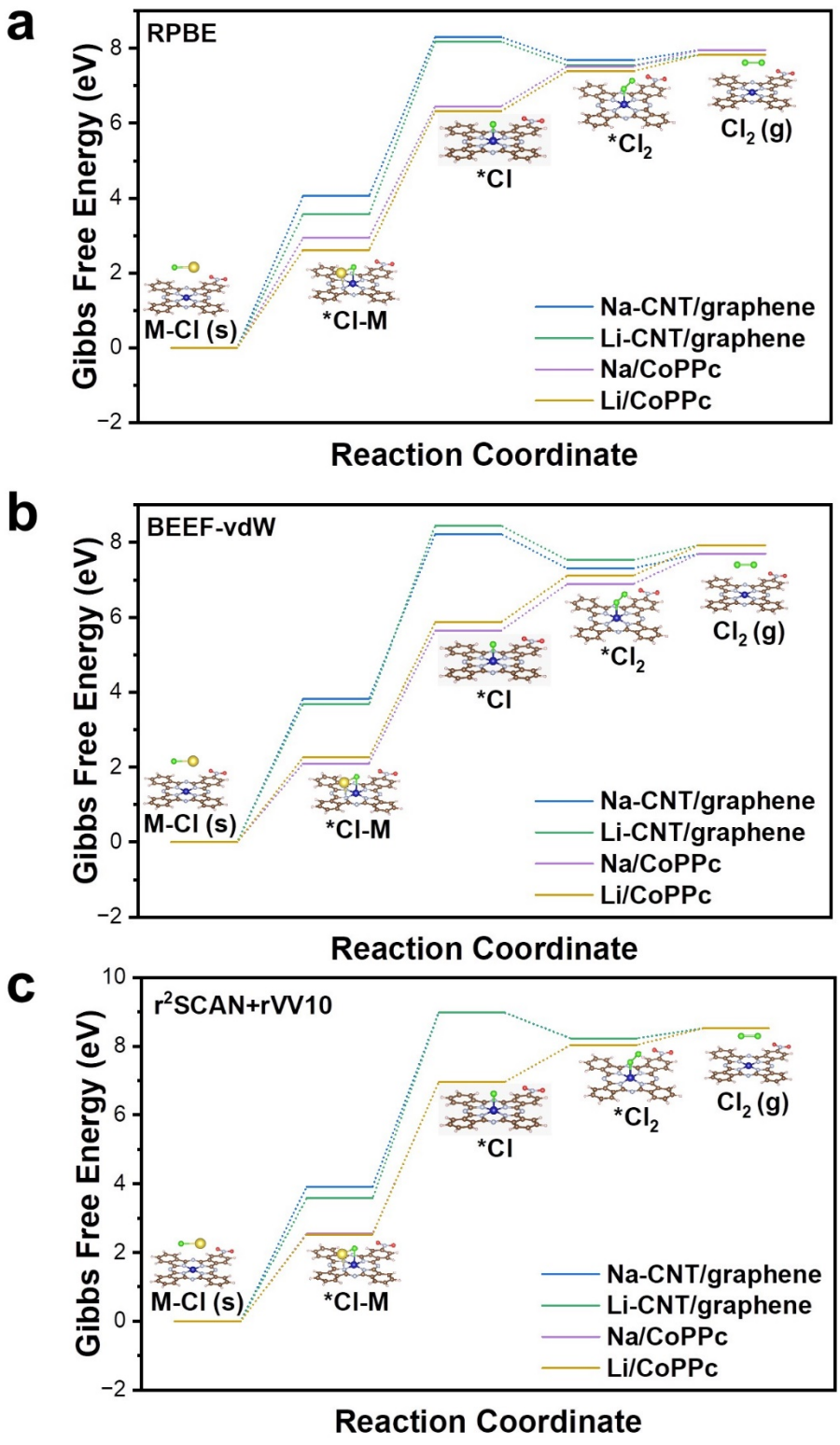

Figure S14. Gibbs free energy changes using different exchange-correlation functionals. a, RPBE. **b,** BEEF-vdW. **c,** r^{2}SCAN+rVV10. Our proposed reaction pathway remained consistent regardless of the functional used.

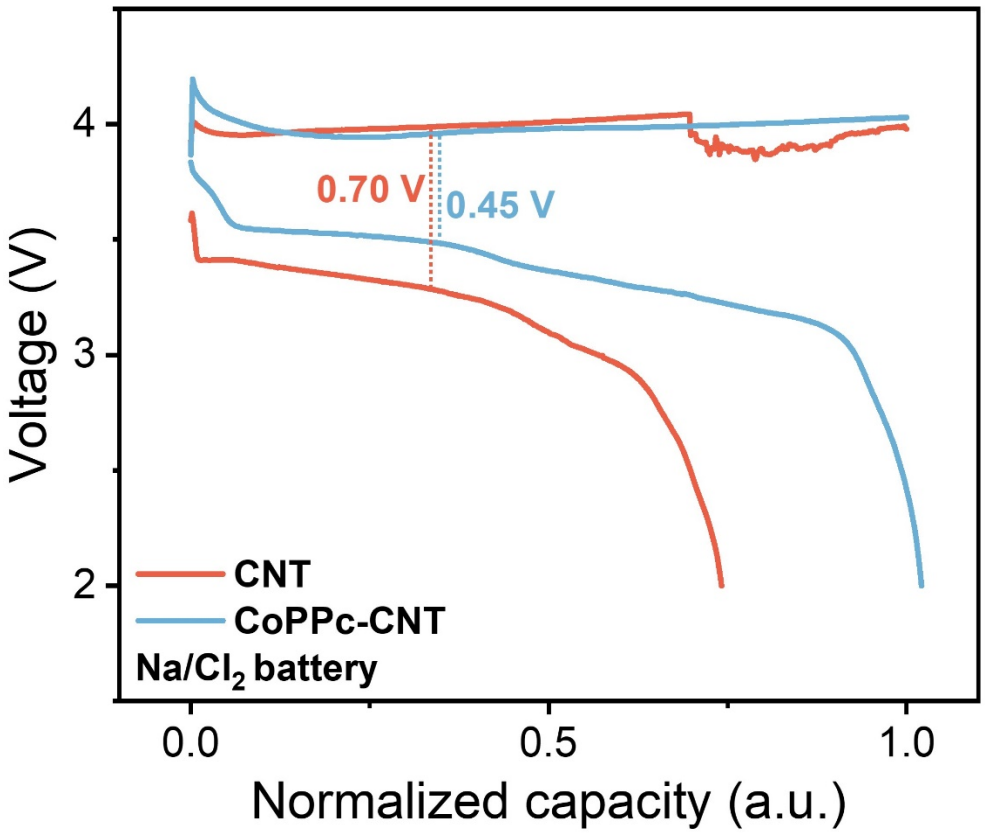

Figure S15. Charge-discharge comparison of Na/Cl_2 batteries using CoPPc-CNT and CNT as the positive electrode. The battery using CoPPc-CNT as the positive electrode had lower overpotential than that using CNT as the positive electrode (lower charging plateau and higher discharging plateau). The capacity in the figure was normalized (maximum charging capacity = 1), so that a better comparison between the two charge-discharge curves could be made.

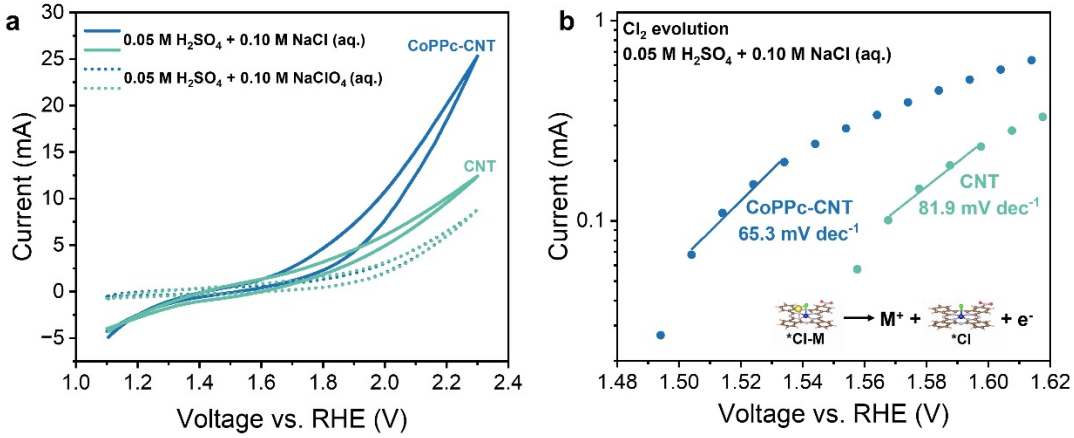

Figure S16. Three-electrode cyclic voltammetry studies of chlorine evolution for CoPPc-CNT and CNT. a, Cyclic voltammetry curves of CoPPc-CNT and CNT in 0.05 M H_2SO_4 + 0.10 M NaCl aqueous solution (chlorine evolution reaction, solid curves) and 0.05 M H_2SO_4 + 0.10 M $NaClO_4$ aqueous solution (oxygen evolution reaction, dotted curves). CoPPc-CNT and CNT demonstrated very similar oxygen evolution reaction performance but showed drastically different chlorine evolution reaction performance. **b,** Tafel slope analysis of chlorine evolution reaction for CoPPc-CNT and CNT. CoPPc-CNT was a better catalyst for chlorine evolution than CNT, with lower onset potential and smaller Tafel slope. The working electrode for the cyclic voltammetry studies was either CoPPc-CNT or CNT loaded on carbon fiber paper. The counter electrode was platinum foil. The reference electrode was reversible hydrogen electrode. The scan rate was 50 mV s^{-1}.

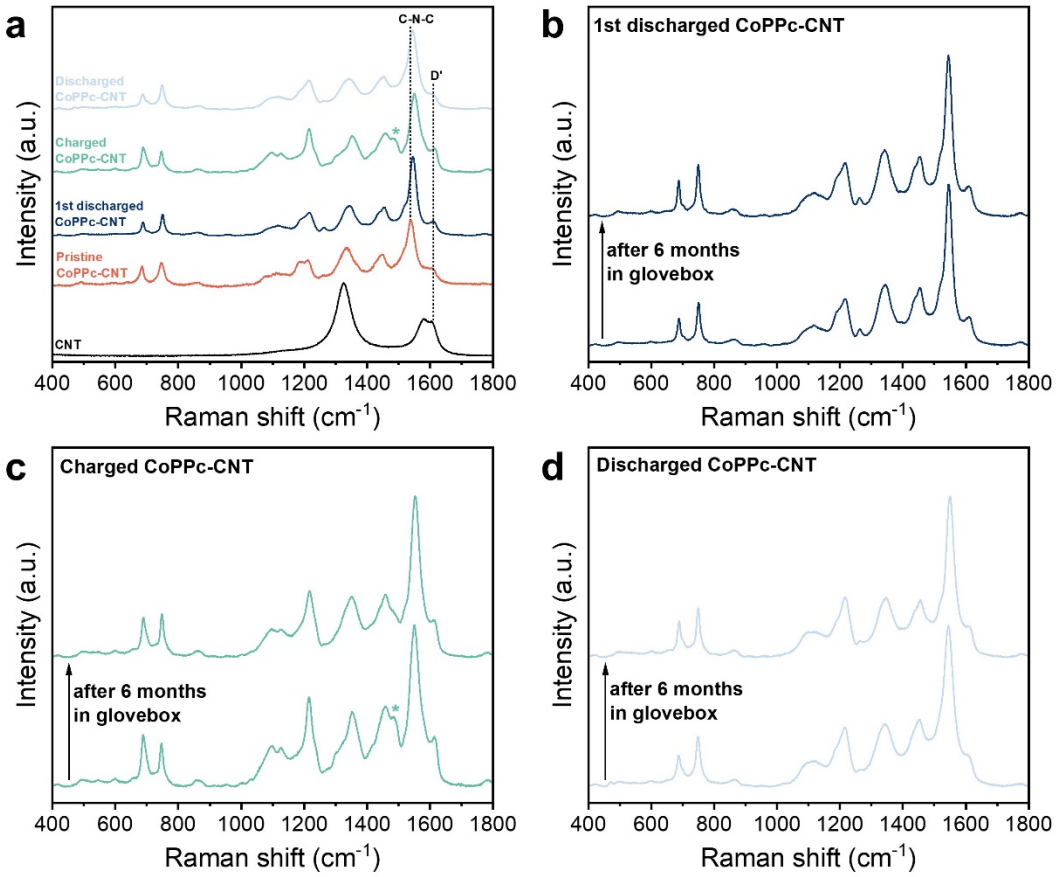

Figure S17. Raman spectra of CNT, pristine CoPPc-CNT, and CoPPc-CNT electrodes stopped at different states during Na/Cl_2 battery cycling. a, Raman spectra of CNT, pristine CoPPc-CNT, and CoPPc-CNT electrodes in Na/Cl_2 battery stopped at different states (after battery's first discharge, after cycled and charged, and after cycled and discharged). **b,** Raman spectra of CoPPc-CNT electrode after the first discharge in Na/Cl_2 battery before and after being stored in an argon-filled glovebox for six months. **c,** Raman spectra of CoPPc-CNT electrode in cycled, charged state during Na/Cl_2 battery cycling before and after being stored in an argon-filled glovebox for six months. **d,** Raman spectra of CoPPc-CNT electrode in cycled, discharged state during Na/Cl_2 battery cycling before and after being stored in an argon-filled glovebox for six months.

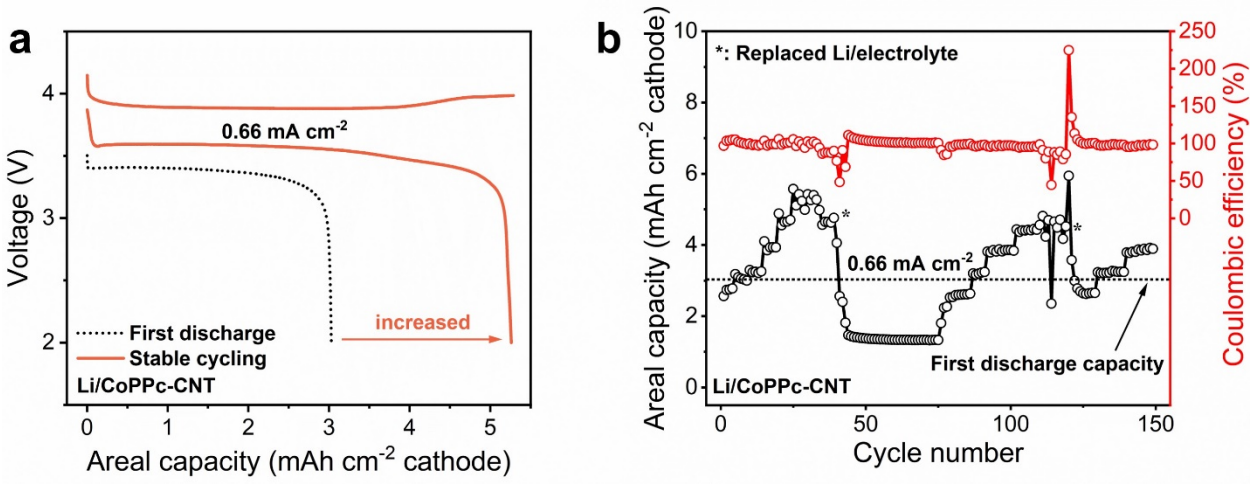

Figure S18. Charge-discharge behavior and cycling performance of Li/Cl_2 battery using CoPPc-CNT as the positive electrode. a, The first discharge curve and charge-discharge behavior of a Li/Cl_2 battery using CoPPc-CNT as the positive electrode. The battery was able to stably cycle at a capacity that was higher than the first discharge capacity. During cycling, the discharge voltage also increased when compared to the first discharge voltage. **b,** Cycling performance of a Li/Cl_2 battery using CoPPc-CNT as the positive electrode. After the coulombic efficiency of the battery began to decay, the cycled CoPPc-CNT positive electrode could pair with a new Li negative electrode and new electrolyte to resume normal cycling. The loading of the CoPPc-CNT in this battery was ~ 6.6 mg cm^{-2}.

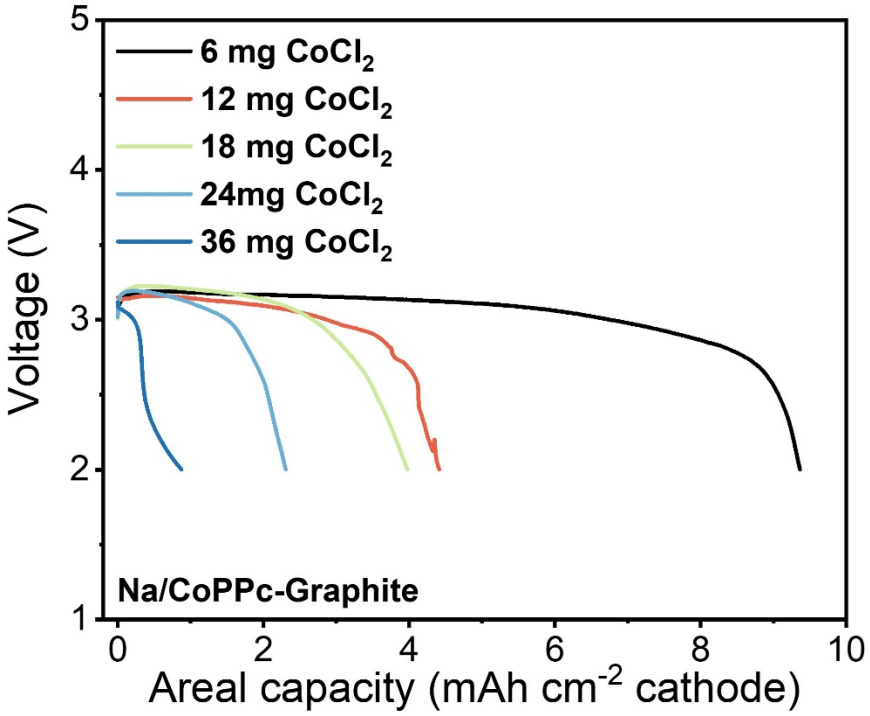

Figure S19. First discharge of Na/Cl_2 battery using CoPPc-Graphite as the positive electrode. The CoPPc-Graphite was synthesized using different amounts of $CoCl_2$ as the starting material. With more CoPPc grown on graphite, the first discharge capacity gradually decreased.

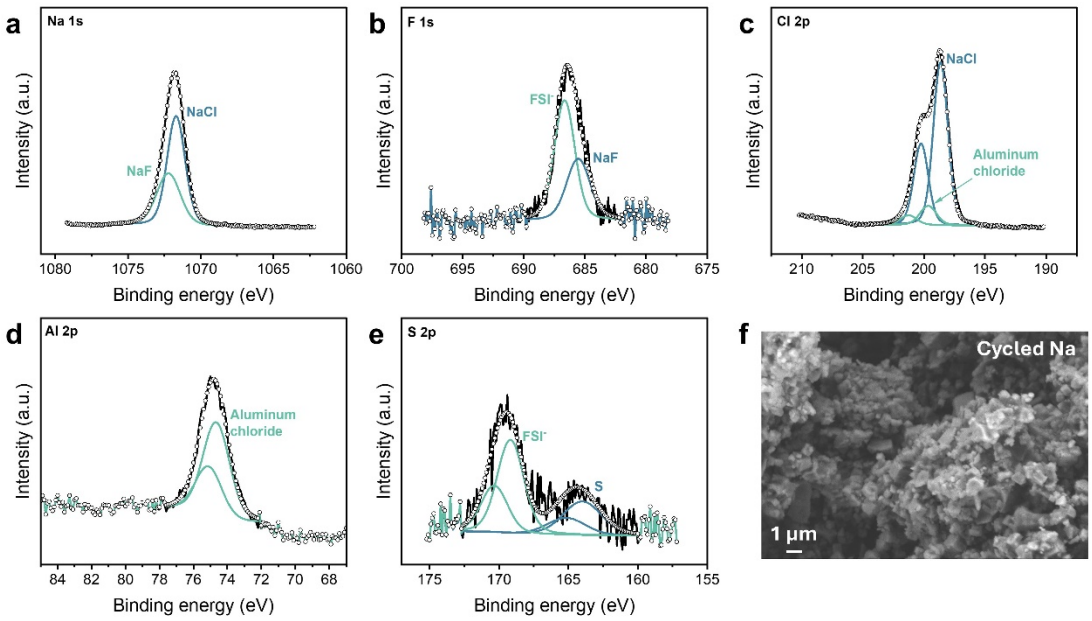

Figure S20. XPS and SEM analysis of the Na negative electrode cycled in a Na/Cl_2 battery. a, Na 1s spectrum of the Na negative electrode. **b,** F 1s spectrum of the Na negative electrode. **c,** Cl 2p spectrum of the Na negative electrode. **d,** Al 2p spectrum of the Na negative electrode. **e,** S 2p spectrum of the Na negative electrode. **f,** SEM image of the Na negative electrode. The solid electrolyte interphase layer was constituted by various components, including sodium chloride, sodium fluoride, aluminum chloride, sulfur, and bis(fluorosulfonyl)imide salts.

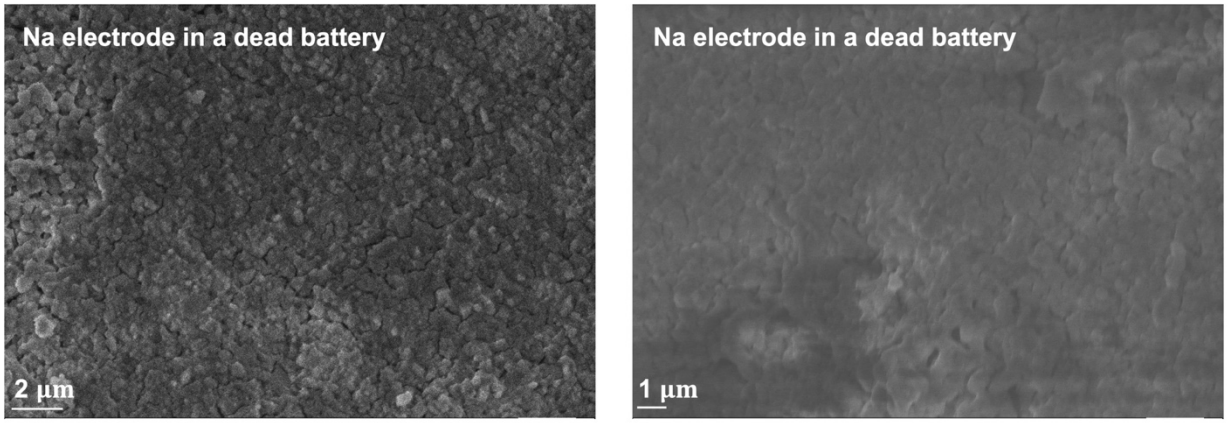

Figure S21. SEM images of Na negative electrode in a dead Na/Cl_2 battery. The Na negative electrode was fully passivated by a thick layer of NaCl crystals, making the electrode insulating and unable to support an efficient Na plating/stripping and facile ions transport.

	Loading (mg cm^{-2})	Cycling capacity/First discharge capacity (Cycle life > 10)
Reference 1	2-4	42.7%
Reference 8	4.3	42.7%
Reference 9	0.7	13.9%
Reference 10	1-2	58.1%
Reference 11	0.8-1.3	63.6%
Reference 12	N/A	24.5%
Reference 18	2	45.2%
Reference 20	1.2	12%
Reference 46	1.5-2	11.4%
CoPPc-CNT for Na/Cl_2	**4.5**	**387%**
CoPPc-CNT for Li/Cl_2	**6.6**	**175%**

Table S5. Comparison of CoPPc-CNT reported in this work with various positive electrodes in previously reported Cl_2 batteries or similar battery systems in terms of loading and the ratio between cycling capacity and first discharge capacity for cycle life > 10. The CoPPc-CNT reported in this work demonstrated clear advantages in both categories. The reference number in this table was according to the reference list in the main manuscript.

References

(1) Hafner, J. Ab-initio simulations of materials using VASP: Density-functional theory and beyond. *Journal of Computational Chemistry* **2008**, *29* (13), 2044-2078. DOI: 10.1002/jcc.21057.
(2) Kresse, G.; Joubert, D. From ultrasoft pseudopotentials to the projector augmented-wave method. *Physical Review B* **1999**, *59* (3), 1758-1775. DOI: 10.1103/PhysRevB.59.1758.
(3) Perdew, J. P.; Burke, K.; Ernzerhof, M. Generalized Gradient Approximation Made Simple. *Physical Review Letters* **1996**, *77* (18), 3865-3868. DOI: 10.1103/PhysRevLett.77.3865.
(4) Grimme, S.; Antony, J.; Ehrlich, S.; Krieg, H. A consistent and accurate ab initio parametrization of density functional dispersion correction (DFT-D) for the 94 elements H-Pu. *The Journal of Chemical Physics* **2010**, *132* (15). DOI: 10.1063/1.3382344.